

# Dominant mixed QCD–electroweak $\mathcal{O}(\alpha_s\alpha)$ corrections to Drell–Yan processes in the resonance region

STEFAN DITTMAYER<sup>1</sup>, ALEXANDER HUSS<sup>2,3</sup>  
AND CHRISTIAN SCHWINN<sup>1,4</sup>

<sup>1</sup> *Albert-Ludwigs-Universität Freiburg, Physikalisches Institut,  
D-79104 Freiburg, Germany*

<sup>2</sup> *Institute for Theoretical Physics, ETH, CH-8093 Zürich, Switzerland*

<sup>3</sup> *Department of Physics, University of Zürich, CH-8057 Zürich, Switzerland*

<sup>4</sup> *Institute for Theoretical Particle Physics and Cosmology,  
RWTH Aachen University, D-52056 Aachen*

## Abstract:

A precise theoretical description of W- and Z-boson production in the resonance region is essential for the correct interpretation of high-precision measurements of the W-boson mass and the effective weak mixing angle. Currently, the largest unknown fixed-order contribution is given by the mixed QCD–electroweak corrections of  $\mathcal{O}(\alpha_s\alpha)$ . We argue, using the framework of the pole expansion for the NNLO QCD–electroweak corrections established in a previous paper, that the numerically dominant corrections arise from the combination of large QCD corrections to the production with the large electroweak corrections to the decay of the W/Z boson. We calculate these so-called factorizable corrections of “initial–final” type and estimate the impact on the W-boson mass extraction. We compare our results to simpler approximate combinations of electroweak and QCD corrections in terms of naive products of NLO QCD and electroweak correction factors and using leading-logarithmic approximations for QED final-state radiation as provided by the structure-function approach or QED parton-shower programs. We also compute corrections of “final–final” type, which are given by finite counterterms to the leptonic vector-boson decays and are found to be numerically negligible.

## 1 Introduction

The class of Drell–Yan-like processes is one of the most prominent types of particle reactions at hadron colliders and describes the production of a lepton pair through an intermediate gauge-boson decay,

$$pp/p\bar{p} \rightarrow V \rightarrow \ell_1 \bar{\ell}_2 + X.$$

Depending on the electric charge of the colour-neutral gauge boson  $V$ , the process can be further classified into the neutral-current ( $V = Z/\gamma$ ) and the charged-current ( $V = W^\pm$ ) processes. The large production rate in combination with the clean experimental signature of the leptonic vector-boson decay allows this process to be measured with great precision. Moreover, the Drell–Yan-like production of  $W$  or  $Z$  bosons is one of the theoretically best understood and most precisely predicted processes. As a consequence, electroweak (EW) gauge-boson production is among the most important “standard-candle” processes at the LHC (see, e.g. Refs. [1, 2]). Its cross section can be used as a luminosity monitor, and the measurement of the mass and width of the  $Z$  boson represents a powerful tool for detector calibration. Furthermore, the  $W$  charge asymmetry and the rapidity distribution of the  $Z$  boson deliver important constraints in the fit of the parton distribution functions (PDFs) [3], which represent crucial ingredients for almost all predictions at the LHC.

Of particular relevance for precision tests of the Standard Model is the potential of the Drell–Yan process at the LHC for high-precision measurements in the resonance regions, where the effective weak mixing angle, quantified by  $\sin^2 \theta_{\text{eff}}^\ell$ , might be extracted from data with LEP precision [4]. The  $W$ -boson mass can be determined from a fit to the distributions of the lepton transverse momentum ( $p_{T,\ell}$ ) and the transverse mass of the lepton pair ( $M_{T,\ell\nu}$ ) which exhibit Jacobian peaks around  $M_W$  and  $M_W/2$ , respectively, and allow for a precise extraction of the mass with a sensitivity below 10 MeV [5, 6] provided that PDF uncertainties can be reduced [7–10].

To fully exploit the potential of the extraordinary experimental precision that is achievable for the Drell–Yan process, it is necessary to have theoretical predictions that match or even surpass the expected accuracy. The current state of the art includes QCD corrections at next-to-next-to-leading-order (NNLO) accuracy [11–18] supplemented by leading higher-order soft-gluon effects [19–22] and soft-gluon resummation for small transverse momenta [23–29]. For event generation, next-to-leading-order (NLO) calculations have been matched to parton showers [30–32], with a recent effort to include NNLO corrections in a parton-shower framework [33–35]. Concerning EW effects, the NLO corrections [36–47] as well as leading higher-order effects from multiple photon emission and universal weak effects [46–50] are known. The sensitivity to the photon PDF through photon-induced production channels has been studied in Refs. [44, 47, 51, 52].

In addition to the  $N^3\text{LO}$  QCD corrections, the next frontier in theoretical fixed-order computations is given by the calculation of the mixed QCD–EW corrections of  $\mathcal{O}(\alpha_s\alpha)$  [53]. These corrections can affect observables relevant for the  $M_W$  determination at the percent level [54] and therefore must be under theoretical control. Up to now, QCD and EW corrections have been combined in various approximations [55–60]. However, a full NNLO calculation at  $\mathcal{O}(\alpha_s\alpha)$  is necessary for a proper combination of QCD and EW corrections without ambiguities. Here some partial results for two-loop amplitudes [61–63] as well as the full  $\mathcal{O}(\alpha_s\alpha)$  corrections to the  $W$  and  $Z$  decay widths [64, 65] are known. A complete calculation of the  $\mathcal{O}(\alpha_s\alpha)$  corrections requires to combine the double-virtual corrections with the  $\mathcal{O}(\alpha)$  EW corrections to  $W/Z + \text{jet}$  production [66–72], the  $\mathcal{O}(\alpha_s)$  QCD corrections to  $W/Z + \gamma$  production [68, 73–81], and the double-real corrections using a method to regularize infrared (IR) singularities.

In a previous paper [82], we have initiated the calculation of the  $\mathcal{O}(\alpha_s\alpha)$  corrections to Drell–Yan processes in the resonance region via the so-called *pole approximation* (PA) [83], which has

been successfully applied to the EW corrections to W production [39, 82, 84, 85] and Z production [82] at NLO. It is based on a systematic expansion of the cross section about the resonance pole and is suitable for theoretical predictions in the vicinity of the gauge-boson resonance, where the higher precision is especially relevant. The PA splits the corrections into distinct well-defined subsets, which can be calculated separately. This allows to assess the numerical impact of different classes of corrections and to identify the dominant contributions. More precisely, the contributions can be classified into two types: the factorizable and the non-factorizable corrections. In the former, the corrections can be separately attributed to the production and the subsequent decay of the gauge boson, whereas in the latter the production and decay subprocesses are linked by the exchange of soft photons. At  $\mathcal{O}(\alpha)$ , the PA shows agreement with the known NLO EW corrections up to fractions of 1% near the resonance, i.e. at a phenomenologically satisfactory level [82]. In particular, the bulk of the NLO EW corrections near the resonance can be attributed to the factorizable corrections to the W/Z decay subprocesses, while the factorizable corrections to the production process are mostly suppressed below the percent level, and the non-factorizable contributions being even smaller.

Based on the quality of the PA at NLO we are confident that this approach is suitable to calculate the  $\mathcal{O}(\alpha_s\alpha)$  corrections with sufficient accuracy for the description of observables that are dominated by the resonances. The non-factorizable corrections comprise the conceptually most challenging contribution to the PA and have been computed at  $\mathcal{O}(\alpha_s\alpha)$  in Ref. [82]. They turn out to be very small and, thus, demonstrate that for phenomenological purposes the  $\mathcal{O}(\alpha_s\alpha)$  corrections can be factorized into terms associated with initial-state and/or final-state corrections and combinations of the two types. In this paper we calculate the factorizable corrections of the type “initial–final”, which combine large QCD corrections to the production with the large EW corrections to the decay of the W/Z boson. Therefore we expect to capture the dominant contribution at  $\mathcal{O}(\alpha_s\alpha)$  to observables relevant for precision physics dominated by the W and Z resonances. We also compute the corrections of “final–final” type, which are given only by finite counterterms to the leptonic vector-boson decay. The remaining factorizable “initial–initial” corrections are expected to deliver only a small contribution and would further require  $\mathcal{O}(\alpha_s\alpha)$ -corrected PDFs for a consistent evaluation, which are however not available. It is all the more important to isolate this contribution in a well-defined manner, as it is accomplished by the PA.

A technical aspect of higher-order calculations involving massless particles is the proper treatment of IR singularities that are associated with configurations involving soft and/or collinear particles. To this end, we use the dipole subtraction formalism [86–89] and its extension for decay processes presented in Ref. [90] for the analytic cancellation of all IR singularities. Although the cancellation of IR singularities in the  $\mathcal{O}(\alpha_s\alpha)$  corrections presented in this work is accomplished by using a combined approach of the techniques developed for NLO calculations, it represents one of the main technical difficulties in the calculation and we devote special attention to its discussion.

This paper is organized as follows: In Section 2 we present the calculation of the initial–final and final–final factorizable corrections. We discuss the construction of an IR-finite final result for the initial–final corrections in detail with a special focus on the treatment of the combined IR singularities of the QCD and EW corrections. Our numerical results are presented in Section 3, where we compare them to different versions of a naive product ansatz obtained by multiplying NLO QCD and EW correction factors, and to a leading-logarithmic treatment of photon radiation as provided by the structure-function approach or QED parton showers such as PHOTOS [91]. We further perform a  $\chi^2$  fit in order to estimate the effect of the NNLO  $\mathcal{O}(\alpha_s\alpha)$  corrections on the measurement of the W-boson mass. A summary is given in Sect. 4.

## 2 Calculation of the dominant $\mathcal{O}(\alpha_s\alpha)$ corrections in pole approximation

In this section we identify and calculate the dominant  $\mathcal{O}(\alpha_s\alpha)$  corrections to the charged-current and neutral-current Drell–Yan processes in the vicinity of an intermediate vector-boson resonance. In Sect. 2.1 we describe the classification of the  $\mathcal{O}(\alpha_s\alpha)$  corrections in the framework of the PA [82]. We identify factorizable contributions of “initial–final” type—i.e. the combination of QCD corrections to vector-boson production with EW corrections to vector-boson decay—as dominant source for corrections to distributions dominated by the vector-boson resonance. The calculation of the building blocks contributing to the initial–final factorizable corrections is performed in Sect. 2.2. In Sect. 2.3 the different building blocks of the initial–final contributions are combined into a formula suitable for numerical evaluation, where all IR singularities are cancelled explicitly. Finally, in Sect. 2.4 we calculate corrections of “final–final” type, which are given by pure counterterm contributions and are numerically small.

### 2.1 Survey of types of $\mathcal{O}(\alpha_s\alpha)$ corrections in pole approximation

The PA for Drell–Yan processes [39,82–85] provides a systematic classification of contributions to Feynman diagrams that are enhanced by the resonant propagator of a vector boson  $V = W, Z$ . The leading corrections in the expansion around the resonance pole arise from factorizable corrections to W/Z production and decay subprocesses, and non-factorizable corrections that link production and decay by soft-photon exchange. The PA separates corrections to production and decay stages in a consistent and gauge-invariant way. This is particularly relevant for the charged-current Drell–Yan process, where photon radiation off the intermediate W boson contributes simultaneously to the corrections to production and decay of a W boson, and to the non-factorizable contributions. Applications of different variants of the PA to NLO EW corrections [39,82,84,85] have been validated by a comparison to the complete EW NLO calculations and show excellent agreement at the order of some 0.1% in kinematic distributions dominated by the resonance region.

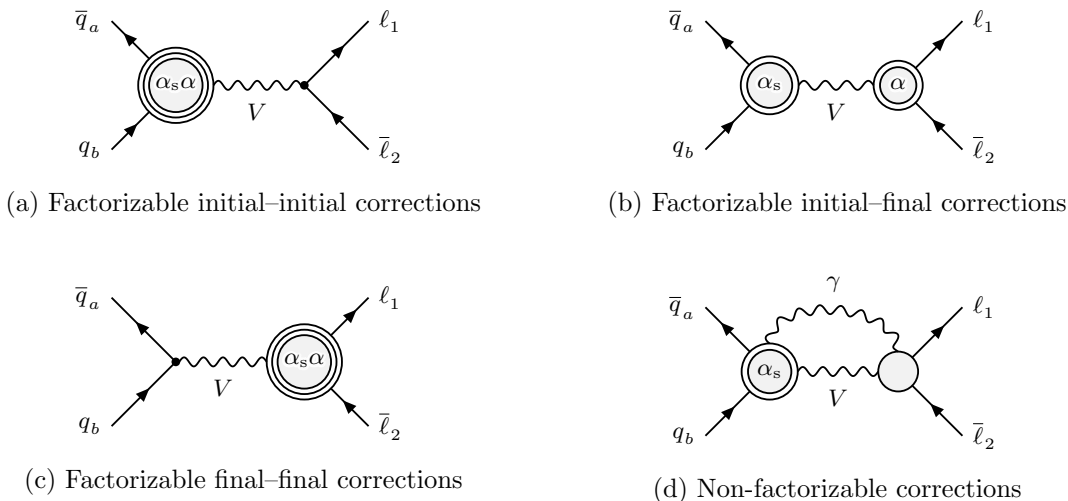


Figure 1: The four types of corrections that contribute to the mixed QCD–EW corrections in the PA illustrated in terms of generic two-loop amplitudes. Simple circles symbolize tree structures, double circles one-loop corrections, and triple circles two-loop contributions.

The structure of the PA for the  $\mathcal{O}(\alpha_s\alpha)$  correction has been worked out in Ref. [82], where details of the method and our setup can be found. The corrections can be classified into the four types of contributions shown in Fig. 1 for the case of the double-virtual corrections. For each class of contributions with the exception of the final-final corrections (c), also the associated real-virtual and double-real corrections have to be computed, obtained by replacing one or both of the labels  $\alpha$  and  $\alpha_s$  in the blobs in Fig. 1 by a real photon or gluon, respectively. The corresponding crossed partonic channels, e.g. with quark-gluon initial states have to be included in addition.

In detail, the four types of corrections are characterized as follows:

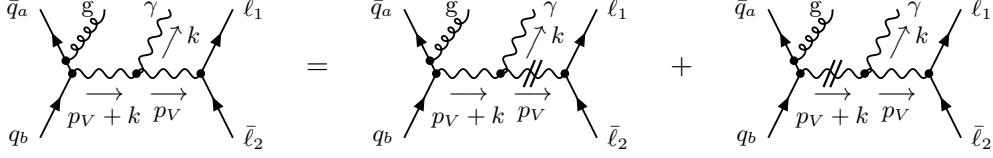
- (a) The initial-initial factorizable corrections are given by two-loop  $\mathcal{O}(\alpha_s\alpha)$  corrections to on-shell  $W/Z$  production and the corresponding one-loop real-virtual and tree-level double-real contributions, i.e.  $W/Z + \text{jet}$  production at  $\mathcal{O}(\alpha)$ ,  $W/Z + \gamma$  production at  $\mathcal{O}(\alpha_s)$ , and the processes  $W/Z + \gamma + \text{jet}$  at tree level. Results for individual ingredients of the initial-initial part are known, such as partial two-loop contributions [61, 63] and the full  $\mathcal{O}(\alpha)$  EW corrections to  $W/Z + \text{jet}$  production including the  $W/Z$  decays [69–71]. However, a consistent combination of these building blocks requires also a subtraction scheme for IR singularities at  $\mathcal{O}(\alpha_s\alpha)$  and has not been performed yet. Note that currently no PDF set including  $\mathcal{O}(\alpha_s\alpha)$  corrections is available, which is required to absorb IR singularities of the initial-initial corrections from photon radiation collinear to the beams.

Results of the PA at  $\mathcal{O}(\alpha)$  show that observables such as the transverse-mass distribution in the case of  $W$  production or the lepton-invariant-mass distributions for  $Z$  production are extremely insensitive to initial-state photon radiation [82]. Since these distributions also receive relatively moderate QCD corrections, we do not expect significant initial-initial NNLO  $\mathcal{O}(\alpha_s\alpha)$  corrections to such distributions. For observables sensitive to initial-state recoil effects, such as the transverse-lepton-momentum distribution, the  $\mathcal{O}(\alpha_s\alpha)$  corrections should be larger, but still very small compared to the huge QCD corrections.<sup>1</sup>

- (b) The factorizable initial-final corrections consist of the  $\mathcal{O}(\alpha_s)$  corrections to  $W/Z$  production combined with the  $\mathcal{O}(\alpha)$  corrections to the leptonic  $W/Z$  decay. Both types of corrections are large and have a sizable impact on the shape of differential distributions at NLO, so that we expect this class of the factorizable corrections to capture the dominant  $\mathcal{O}(\alpha_s\alpha)$  effects. The computation of these contributions is the main result of this paper and is discussed in Sect. 2.2. Preliminary numerical results of these corrections were presented in Refs. [92, 93].
- (c) Factorizable final-final corrections arise from the  $\mathcal{O}(\alpha_s\alpha)$  counterterms of the lepton- $W/Z$ -vertices, which involve only QCD corrections to the vector-boson self-energies. There are no corresponding real contributions, so that the final-final corrections have practically no impact on the shape of distributions. We compute these corrections in Sect. 2.4 below and confirm the expectation that they are phenomenologically negligible.
- (d) The non-factorizable  $\mathcal{O}(\alpha_s\alpha)$  corrections are given by soft-photon corrections connecting the initial state, the intermediate vector boson, and the final-state leptons, combined with QCD corrections to  $V$ -boson production. As shown in detail in Ref. [82], these corrections

---

<sup>1</sup>Note that for such observables a fixed-order QCD description is not adequate near the Jacobian peak, so that in this case the initial-initial corrections need to be combined with a resummation of multiple gluon emissions. At present, such a resummation is available in the POWHEG framework in combination with an approximation to the double-real and real-virtual part of the initial-initial corrections where the first emitted photon or gluon is treated exactly, while further emissions are generated in the collinear approximation [58, 60].



(a) Decomposition of a diagram with photon emission off a  $V$ -boson line into initial–initial and initial–final corrections



(b) Photon emission from the production subprocess      (c) Photon emission from the decay subprocess

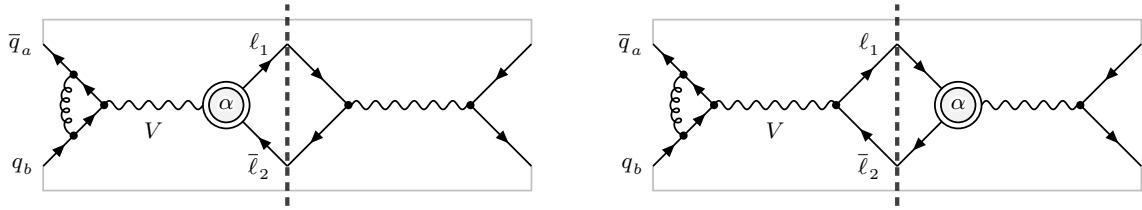
Figure 2: Decomposition of the double-real corrections  $\bar{q}_a(p_a)q_b(p_b) \rightarrow \ell_1(k_1)\bar{\ell}_2(k_2)g(k_g)\gamma(k)$  into initial–initial (b) and initial–final (c) parts, illustrated for an example in part (a). The momentum  $p_V$  of the intermediate vector boson  $V$  is given by  $p_V = p_a + p_b - k_g - k = k_1 + k_2$ . A double line on a  $V$  propagator indicates on-shellness while a gauge boson attached to an encircled subdiagram indicates all possible insertions.

can be expressed in terms of soft-photon correction factors to squared tree-level or one-loop QCD matrix elements by using gauge-invariance arguments. The numerical impact of these corrections was found to be below the 0.1% level and is therefore negligible for all phenomenological purposes.

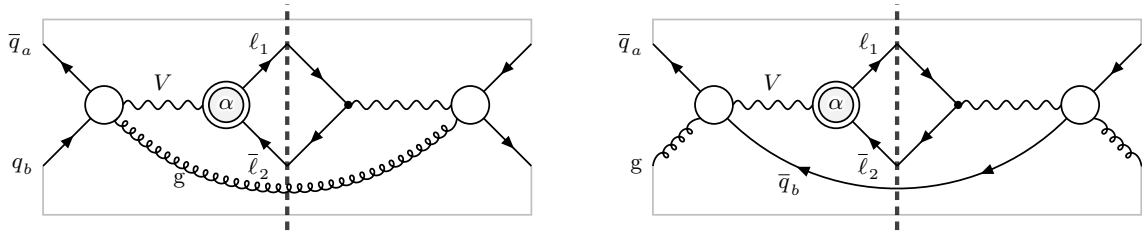
The definition of the factorizable corrections and the separation of initial- and final-state corrections is illustrated in Fig. 2 for the case of the double-real corrections. An example diagram for the charged-current process is given in Fig. 2a, which cannot be attributed uniquely to the vector-boson production or decay subprocess and displays an overlapping resonance structure due to the propagator poles at  $p_V^2 = \mu_V^2$  and  $(p_V + k)^2 = \mu_V^2$ . Here  $\mu_V$  combines the real mass and width parameters of  $V$ ,  $M_V$  and  $\Gamma_V$ , to a complex mass value,  $\mu_V^2 = M_V^2 - iM_V\Gamma_V$ . However, a simple partial-fractioning identity for the two  $V$ -boson propagators allows us to disentangle the two resonance structures and to decompose such diagrams into contributions associated with photon emission from the production or decay subprocesses of an on-shell  $V$  boson (see Eq. (2.11) in Ref. [82]). This is illustrated in Fig. 2a, where the double slash on a propagator line indicates that the corresponding momentum is set on its mass shell in the rest of the diagram (but not on the slashed line itself). Using this decomposition, the double-real corrections can be divided consistently into initial–initial and initial–final contributions, as shown in Fig. 2b and Fig. 2c, respectively. Here a diagrammatic notation is used where an encircled diagram with an attached photon or gluon stands for all possibilities to attach the photon/gluon to the fermion line and the gauge boson  $V$  (see Eq. (2.12) in Ref. [82] for an example). The initial–final (virtual QCD)  $\times$  (real EW) corrections are treated analogously. All different contributions to the factorizable initial–final corrections are diagrammatically characterized in terms of interference diagrams in Fig. 3.

## 2.2 Calculation of the factorizable initial–final corrections

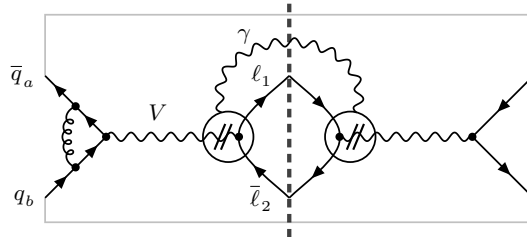
In this section we calculate the various contributions to the factorizable initial–final corrections of  $\mathcal{O}(\alpha_s\alpha)$  shown in Fig. 3. Most contributions can be expressed in terms of reducible



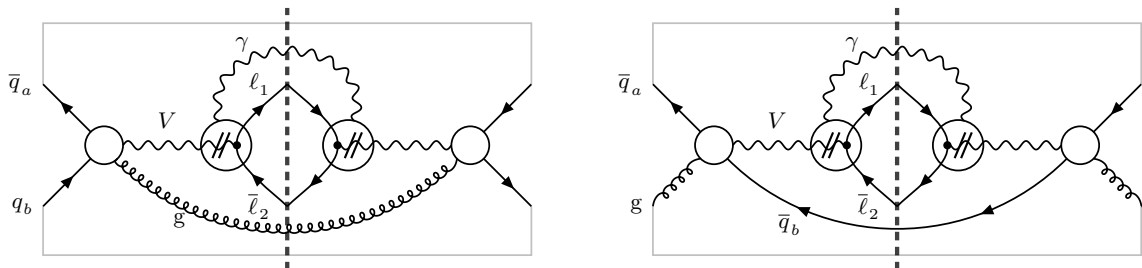
(a) Factorizable initial-final double-virtual corrections



(b) Factorizable initial-final (real QCD) $\times$ (virtual EW) corrections



(c) Factorizable initial-final (virtual QCD) $\times$ (real photonic) corrections



(d) Factorizable initial-final double-real corrections

Figure 3: Interference diagrams for the various contributions to the factorizable initial-final corrections of  $\mathcal{O}(\alpha_s\alpha)$ , with blobs representing all relevant tree structures. The blobs with “ $\alpha$ ” inside represent one-loop corrections of  $\mathcal{O}(\alpha)$ .

products of NLO QCD and NLO EW building blocks. For details on the notation used for these NLO results we refer to Ref. [82].

### 2.2.1 Double-virtual corrections

The double-virtual  $\mathcal{O}(\alpha_s\alpha)$  initial-final corrections to the squared  $\bar{q}_a q_b \rightarrow \ell_1 \bar{\ell}_2$  amplitude are illustrated in Fig. 3(a) in terms of interference diagrams. They arise in two ways: from the interference of the tree amplitude with the two-loop  $\mathcal{O}(\alpha_s\alpha)$  amplitude and from the interference between the one-loop amplitudes with  $\mathcal{O}(\alpha_s)$  corrections to  $V$ -boson production and  $\mathcal{O}(\alpha)$  corrections to the decay, respectively,

$$\begin{aligned} |\mathcal{M}_{\bar{q}_a q_b \rightarrow \ell_1 \bar{\ell}_2}|^2 \Big|_{\text{prod} \times \text{dec}}^{\text{V}_s \otimes \text{V}_{\text{ew}}} &= 2 \text{Re} \left\{ \delta \mathcal{M}_{\text{V}_s \otimes \text{V}_{\text{ew}}, \text{prod} \times \text{dec}}^{\bar{q}_a q_b \rightarrow \ell_1 \bar{\ell}_2} \left( \mathcal{M}_{0, \text{PA}}^{\bar{q}_a q_b \rightarrow \ell_1 \bar{\ell}_2} \right)^* \right\} \\ &+ 2 \text{Re} \left\{ \delta \mathcal{M}_{\text{V}_{\text{ew}}, \text{dec}}^{\bar{q}_a q_b \rightarrow \ell_1 \bar{\ell}_2} \left( \delta \mathcal{M}_{\text{V}_s, \text{PA}}^{\bar{q}_a q_b \rightarrow \ell_1 \bar{\ell}_2} \right)^* \right\}. \end{aligned} \quad (2.1)$$

The LO amplitude in PA,  $\mathcal{M}_{0, \text{PA}}$ , differs from the full LO matrix element by the absence of the non-resonant photon diagram in case of the neutral-current Drell-Yan process. The first term on the right-hand side in Eq. (2.1) involves the factorizable initial-final contribution to the two-loop amplitude, which takes the form of reducible (one-loop)  $\times$  (one-loop) diagrams and is defined explicitly as

$$\delta \mathcal{M}_{\text{V}_s \otimes \text{V}_{\text{ew}}, \text{prod} \times \text{dec}}^{\bar{q}_a q_b \rightarrow \ell_1 \bar{\ell}_2} = \sum_{\lambda_V} \frac{\delta \mathcal{M}_{\text{V}_s}^{\bar{q}_a q_b \rightarrow V}(\lambda_V) \delta \mathcal{M}_{\text{V}_{\text{ew}}}^{V \rightarrow \ell_1 \bar{\ell}_2}(\lambda_V)}{p_V^2 - \mu_V^2} = \delta_{\text{V}_s}^{\text{V} \bar{q}_a q_b} \delta_{\text{V}_{\text{ew}}}^{\text{dec}} \mathcal{M}_{0, \text{PA}}^{\bar{q}_a q_b \rightarrow \ell_1 \bar{\ell}_2}, \quad (2.2)$$

where a sum over the physical polarization states of the vector boson  $V$ , labelled by  $\lambda_V$ , is performed. In the second step in Eq. (2.2) the fact is used that the one-loop corrections to the production and decay factorize off the corresponding LO matrix elements,

$$\delta \mathcal{M}_{\text{V}_s}^{\bar{q}_a q_b \rightarrow V} = \delta_{\text{V}_s}^{\text{V} \bar{q}_a q_b} \mathcal{M}_0^{\bar{q}_a q_b \rightarrow V}, \quad (2.3)$$

$$\delta \mathcal{M}_{\text{V}_{\text{ew}}, \text{dec}}^{V \rightarrow \ell_1 \bar{\ell}_2} = \delta_{\text{V}_{\text{ew}}}^{\text{dec}} \mathcal{M}_{0, \text{PA}}^{V \rightarrow \ell_1 \bar{\ell}_2}. \quad (2.4)$$

The virtual QCD corrections are well known and are quoted explicitly in Eq. (2.35) of Ref. [82]. The explicit expressions for the NLO EW correction factors can be found, e.g., in Refs. [39, 47], and are quoted in Appendix B.2 of Ref. [93]. In order to maintain gauge invariance, the NLO production and decay subamplitudes in Eq. (2.2), and in particular the correction factor  $\delta_{\text{V}_{\text{ew}}}^{\text{dec}}$ , are evaluated for on-shell  $V$  bosons. We keep the QCD correction factor  $\delta_{\text{V}_s}^{\text{V} \bar{q}_a q_b}$  off shell, i.e. without setting  $s \rightarrow M_V^2$  there to be closer to the full calculation, which is possible, because  $\delta_{\text{V}_s}^{\text{V} \bar{q}_a q_b}$  does not depend on  $M_V$  at all. The on-shell projection  $s \rightarrow M_V^2$  in the EW correction involves some freedom, but numerical effects from different implementations are of the same order as the intrinsic uncertainty of the PA. However, the choice of the mappings in the virtual and real corrections has to match properly in order to ensure the correct cancellation of IR singularities.

The expressions (2.3) and (2.4) also enter the one-loop interference terms in the second line of Eq. (2.1). The final result for the double-virtual corrections to the cross section is therefore given by

$$\begin{aligned} d\sigma_{\bar{q}_a q_b, \text{prod} \times \text{dec}}^{\text{V}_s \otimes \text{V}_{\text{ew}}} &= 2 \left[ \text{Re} \left\{ \delta_{\text{V}_{\text{ew}}}^{\text{dec}} \delta_{\text{V}_s}^{\text{V} \bar{q}_a q_b} \right\} + \text{Re} \left\{ \delta_{\text{V}_{\text{ew}}}^{\text{dec}} \left( \delta_{\text{V}_s}^{\text{V} \bar{q}_a q_b} \right)^* \right\} \right] d\sigma_{\bar{q}_a q_b, \text{PA}}^0 \\ &= 4 \text{Re} \left\{ \delta_{\text{V}_{\text{ew}}}^{\text{dec}} \right\} \text{Re} \left\{ \delta_{\text{V}_s}^{\text{V} \bar{q}_a q_b} \right\} d\sigma_{\bar{q}_a q_b, \text{PA}}^0. \end{aligned} \quad (2.5)$$



Both the EW and QCD correction factors contain soft and collinear singularities, which take the form of  $\frac{1}{\epsilon^2}$  poles for massless fermions. Therefore, in principle, Eq. (2.5) requires the evaluation of the correction factors up to  $\mathcal{O}(\epsilon^2)$  in order to obtain all finite  $\mathcal{O}(\epsilon^0)$  terms. However, after applying the subtraction formalism, which we describe in detail in Sect. 2.3, the poles are cancelled before performing the full expansion in  $\epsilon$  and, thus, the results up to order  $\mathcal{O}(\epsilon^0)$  turn out to be sufficient. This result is obvious if the soft and collinear singularities are not regularized in  $D = 4 - 2\epsilon$  dimensions, but by small mass parameters, where no rational terms from the multiplication of  $1/\epsilon$  poles with  $D$ -dimensional quantities exist at all.

### 2.2.2 (Real QCD) $\times$ (virtual EW) corrections

The (real QCD)  $\times$  (virtual EW) contributions to the factorizable initial–final corrections shown in Fig. 3(b) arise by including the virtual corrections to the leptonic W/Z decays to the various partonic subprocesses of  $V + \text{jet}$  production,

$$\bar{q}_a(p_a) + q_b(p_b) \rightarrow V(p_V) + g(k_g), \quad (2.6a)$$

$$g(p_g) + q_b(p_b) \rightarrow V(p_V) + q_a(k_a), \quad (2.6b)$$

$$g(p_g) + \bar{q}_a(p_a) \rightarrow V(p_V) + \bar{q}_b(k_b). \quad (2.6c)$$

For the quark-induced channel, the corrections are given by replacing the virtual QCD amplitude in Eq. (2.2) by the corresponding amplitude for real-gluon emission,

$$\delta\mathcal{M}_{R_s \otimes V_{\text{ew}}, \text{prod} \times \text{dec}}^{\bar{q}_a q_b \rightarrow \ell_1 \bar{\ell}_2 g} = \sum_{\lambda_V} \frac{\mathcal{M}_{R_s}^{\bar{q}_a q_b \rightarrow g V}(\lambda_V) \delta\mathcal{M}_{V_{\text{ew}}}^{V \rightarrow \ell_1 \bar{\ell}_2}(\lambda_V)}{p_V^2 - \mu_V^2}. \quad (2.7)$$

Analogously to the double-virtual case, the EW decay subamplitude is evaluated for on-shell vector bosons, while the QCD correction is kept off shell. Using the factorization property of the EW one-loop decay corrections (2.4), the (real QCD)  $\times$  (virtual EW) correction to the cross section in the quark–anti-quark channel is proportional to the real NLO QCD corrections  $d\sigma^{R_s}$ ,

$$d\sigma_{\bar{q}_a q_b, \text{prod} \times \text{dec}}^{R_s \otimes V_{\text{ew}}} = 2 \text{Re} \left\{ \delta_{V_{\text{ew}}}^{\text{dec}} \right\} d\sigma_{\bar{q}_a q_b, \text{PA}}^{R_s}. \quad (2.8)$$

As for the Born amplitude, the label PA in the real-emission corrections indicates that all non-resonant terms, i.e. the photon-exchange diagrams in case of the neutral-current process, are omitted in the QCD real-emission amplitudes. Analogous expressions hold for the gluon–quark and gluon–anti-quark initiated subprocesses to  $V + \text{jet}$  production.

### 2.2.3 (Virtual QCD) $\times$ (real photonic) corrections

The (virtual QCD)  $\times$  (real photonic) factorizable corrections of initial–final type arise from the generic interference diagram shown in Fig. 3(c). They are obtained by combining the real-photon corrections to on-shell  $V$ -boson decay with the virtual QCD corrections to  $V$ -boson production,

$$\mathcal{M}_{V_s \otimes R_{\text{ew}}, \text{prod} \times \text{dec}}^{\bar{q}_a q_b \rightarrow \ell_1 \bar{\ell}_2 \gamma} = \sum_{\lambda_V} \frac{\delta\mathcal{M}_{V_s}^{\bar{q}_a q_b \rightarrow V}(\lambda_V) \mathcal{M}_{R_{\text{ew}}}^{V \rightarrow \ell_1 \bar{\ell}_2 \gamma}(\lambda_V)}{(p_V + k)^2 - \mu_V^2} = \delta_{V_s}^{V \bar{q}_a q_b} \mathcal{M}_{R_{\text{ew}}, \text{fact}, \text{dec}}^{\bar{q}_a q_b \rightarrow \ell_1 \bar{\ell}_2 \gamma}. \quad (2.9)$$

In the second step, Eq. (2.3) has been used to factorize the virtual QCD correction factor from the matrix element  $\mathcal{M}_{R_{\text{ew}}, \text{fact}, \text{dec}}^{\bar{q}_a q_b \rightarrow \ell_1 \bar{\ell}_2 \gamma}$  for the factorizable NLO decay corrections (see Eq. (2.14) in Ref [82]). Again the matrix elements for the EW decay subprocess is evaluated for on-shell vector

bosons, while the QCD correction factor is kept off shell. As illustrated in Fig. 2 and discussed in detail in Ref. [82], the splitting of photon-emission effects off the intermediate  $V$ -boson into parts corresponding to initial- or final-state radiation separates the two resonance propagator factors  $1/(p_V^2 - M_V^2)$  and  $1/[(p_V^2 + k)^2 - M_V^2]$ , respectively, where  $p_V = k_1 + k_2$ . For factorizable EW decay correction we, thus, have to perform the on-shell projection  $(p_V^2 + k)^2 \rightarrow M_V^2$ . The resulting contribution of the (virtual QCD)  $\times$  (real photonic) corrections to the cross section therefore assumes the form

$$d\sigma_{\bar{q}_a q_b, \text{prod} \times \text{dec}}^{\text{Vs} \otimes \text{R}_{\text{ew}}} = 2 \text{Re} \left\{ \delta_{\text{Vs}}^{V \bar{q}_a q_b} \right\} d\sigma_{\bar{q}_a q_b, \text{dec}}^{\text{R}_{\text{ew}}}. \quad (2.10)$$

#### 2.2.4 Double-real corrections

The double-real emission corrections are illustrated by interference diagrams in Fig. 3(d) and are defined by the real-emission matrix elements for the  $V + \text{jet}$  production subprocesses (2.6) with the subsequent decay  $V \rightarrow \ell_1 \bar{\ell}_2 \gamma$ ,

$$\mathcal{M}_{\text{R}_s \otimes \text{R}_{\text{ew}}, \text{prod} \times \text{dec}}^{\bar{q}_a q_b \rightarrow \ell_1 \bar{\ell}_2 \gamma g} = \sum_{\lambda_V} \frac{\mathcal{M}_{\text{R}_s}^{\bar{q}_a q_b \rightarrow V g}(\lambda_V) \mathcal{M}_{\text{R}_{\text{ew}}}^{V \rightarrow \ell_1 \bar{\ell}_2 \gamma}(\lambda_V)}{(p_V + k)^2 - \mu_V^2}, \quad (2.11)$$

with analogous expressions for the  $gq$  and  $g\bar{q}$  channels. The non-resonant contribution arising from the case  $V = \gamma$  in the neutral-current process is again not included. Compact explicit results for the helicity amplitudes of the double-real corrections can be found in Ref. [93]. The double-real contribution to the cross section,  $d\sigma_{\text{prod} \times \text{dec}}^{\text{R}_s \otimes \text{R}_{\text{ew}}}$ , is defined in terms of the square of the matrix element (2.11) where the decay subamplitudes are evaluated for on-shell  $V$  bosons. Due to the spin correlations of the production and decay matrix elements and the full kinematics of the  $2 \rightarrow 4$  scattering process, the double-real corrections do not factorize further into separate EW and QCD correction factors, in contrast to the other classes of factorizable initial–final corrections.

### 2.3 Treatment of infrared singularities for the factorizable initial–final corrections

The NNLO  $\mathcal{O}(\alpha_s \alpha)$  contributions to the cross section due to the factorizable initial–final corrections are obtained by integrating the four contributions discussed in the previous section over the respective phase spaces,

$$\begin{aligned} \hat{\sigma}_{\text{prod} \times \text{dec}}^{\text{NNLO}_{\text{s} \otimes \text{ew}}} &= \int_2 d\sigma_{\text{prod} \times \text{dec}}^{\text{Vs} \otimes \text{V}_{\text{ew}}} + \iint_{2+\gamma} d\sigma_{\text{prod} \times \text{dec}}^{\text{Vs} \otimes \text{R}_{\text{ew}}} + \int_3 d\sigma_{\text{prod} \times \text{dec}}^{\text{R}_s \otimes \text{V}_{\text{ew}}} + \iint_{3+\gamma} d\sigma_{\text{prod} \times \text{dec}}^{\text{R}_s \otimes \text{R}_{\text{ew}}} \\ &+ \int_2 d\sigma_{\text{prod} \times \text{dec}}^{\text{Cs} \otimes \text{V}_{\text{ew}}} + \iint_{2+\gamma} d\sigma_{\text{prod} \times \text{dec}}^{\text{Cs} \otimes \text{R}_{\text{ew}}}, \end{aligned} \quad (2.12)$$

where the additional QCD collinear counterterms in the last line were introduced to absorb the collinear singularities associated with the quarks and gluons in the initial state into the NLO PDFs. Note that the EW corrections are completely confined to the decay subprocess, and consequently, there are no singularities from initial-state collinear quark–photon splittings. This allows us to obtain the collinear counterterms in the last line of Eq. (2.12) from the customary

NLO QCD collinear counterterms  $d\sigma^{C_s}$  [86] by replacing the LO cross sections by the appropriate real or virtual EW decay corrections in the PA. Using the results of Sect. 2.2 we can write

$$\begin{aligned}
\hat{\sigma}_{\text{prod}\times\text{dec}}^{\text{NNLO}_{s\otimes\text{ew}}} &= \int_2 4 \text{Re}\left\{\delta_{V_s}^{V\bar{q}_a q_b}\right\} \text{Re}\left\{\delta_{V_{\text{ew}}}^{\text{dec}}\right\} d\sigma_{\text{PA}}^0 + \iint_{2+\gamma} 2 \text{Re}\left\{\delta_{V_s}^{V\bar{q}_a q_b}\right\} d\sigma_{\text{dec}}^{\text{R}_{\text{ew}}} \\
&+ \int_3 2 \text{Re}\left\{\delta_{V_{\text{ew}}}^{\text{dec}}\right\} d\sigma_{\text{PA}}^{\text{R}_s} + \iint_{3+\gamma} d\sigma_{\text{prod}\times\text{dec}}^{\text{R}_s\otimes\text{R}_{\text{ew}}} \\
&+ \int_2 2 \text{Re}\left\{\delta_{V_{\text{ew}}}^{\text{dec}}\right\} d\sigma_{\text{PA}}^{C_s} + \iint_{2+\gamma} d\sigma_{\text{prod}\times\text{dec}}^{C_s\otimes\text{R}_{\text{ew}}}. \tag{2.13}
\end{aligned}$$

Applying the QCD dipole subtraction formalism [86] in order to cancel the IR singularities associated with the QCD corrections, Eq. (2.13) can be written in the following form,

$$\begin{aligned}
\hat{\sigma}_{\text{prod}\times\text{dec}}^{\text{NNLO}_{s\otimes\text{ew}}} &= \int_2 2 \text{Re}\left\{\delta_{V_{\text{ew}}}^{\text{dec}}\right\} d\sigma_{\text{PA}}^0 \otimes \left[2 \text{Re}\left\{\delta_{V_s}^{V\bar{q}_a q_b}\right\} + \mathbf{I}\right] \\
&+ \iint_{2+\gamma} d\sigma_{\text{dec}}^{\text{R}_{\text{ew}}} \otimes \left[2 \text{Re}\left\{\delta_{V_s}^{V\bar{q}_a q_b}\right\} + \mathbf{I}\right] \\
&+ \int_3 2 \text{Re}\left\{\delta_{V_{\text{ew}}}^{\text{dec}}\right\} \left\{d\sigma_{\text{PA}}^{\text{R}_s} - \sum_{\substack{\text{QCD} \\ \text{dipoles}}} d\sigma_{\text{PA}}^0 \otimes dV_{\text{dip}}\right\} \\
&+ \iint_{3+\gamma} \left\{d\sigma_{\text{prod}\times\text{dec}}^{\text{R}_s\otimes\text{R}_{\text{ew}}} - \sum_{\substack{\text{QCD} \\ \text{dipoles}}} d\sigma_{\text{dec}}^{\text{R}_{\text{ew}}} \otimes dV_{\text{dip}}\right\} \\
&+ \int_0^1 dx \int_2 2 \text{Re}\left\{\delta_{V_{\text{ew}}}^{\text{dec}}\right\} d\sigma_{\text{PA}}^0 \otimes (\mathbf{K} + \mathbf{P}) \\
&+ \int_0^1 dx \iint_{2+\gamma} d\sigma_{\text{dec}}^{\text{R}_{\text{ew}}} \otimes (\mathbf{K} + \mathbf{P}). \tag{2.14}
\end{aligned}$$

The explicit expressions of the dipole operators  $dV_{\text{dip}}$  and the insertion operators  $\mathbf{I}$ ,  $\mathbf{K}$ , and  $\mathbf{P}$  can be found in Ref. [86]. The symbol  $\otimes$  denotes possible additional helicity and colour correlations, and it is implicitly assumed that the cross sections multiplying the dipole operators  $dV_{\text{dip}}$  are evaluated on the respective dipole-mapped phase-space point. The explicit expressions associated with the NLO QCD corrections were given in Ref. [82].

All individual integrals appearing in Eq. (2.14) are now free of QCD singularities, but remain IR divergent owing to the singularities contained in the EW corrections which still need to be cancelled between the virtual corrections and the corresponding real-photon-emission parts. For this purpose we employ the dipole subtraction formalism for photon radiation [87, 89], in particular the extension of the formalism to treat decay kinematics described in detail in Ref. [90]. As a result, we are able to arrange the six contributions in Eq. (2.14) into a form where all IR divergences are cancelled in the integrands explicitly,

$$\hat{\sigma}_{\text{prod}\times\text{dec}}^{\text{NNLO}_{s\otimes\text{ew}}} = \tilde{\sigma}_{\text{prod}\times\text{dec}}^{V_s\otimes V_{\text{ew}}} + \tilde{\sigma}_{\text{prod}\times\text{dec}}^{V_s\otimes\text{R}_{\text{ew}}} + \tilde{\sigma}_{\text{prod}\times\text{dec}}^{\text{R}_s\otimes V_{\text{ew}}} + \tilde{\sigma}_{\text{prod}\times\text{dec}}^{\text{R}_s\otimes\text{R}_{\text{ew}}} + \tilde{\sigma}_{\text{prod}\times\text{dec}}^{C_s\otimes V_{\text{ew}}} + \tilde{\sigma}_{\text{prod}\times\text{dec}}^{C_s\otimes\text{R}_{\text{ew}}}, \tag{2.15}$$

where each term is an IR-finite object and its phase-space integration can be performed numerically in four dimensions. Equation (2.15) is our master formula for the numerical evaluation

discussed in Sect. 3. Explicit expressions for all contributions for the quark–anti-quark and quark–gluon induced channels are given in Appendix B.

The first two terms in Eq. (2.15) arise from the sum of the double-virtual and the (virtual QCD)×(real photonic) corrections, including the insertion operators from the QCD dipole formalism, and correspond to the sum of the first two lines in Eq. (2.14). Applying the dipole formalism to rearrange the IR singularities of photonic origin between the virtual and real EW corrections, we obtain the following expressions for the IR-finite virtual QCD contributions to the cross section,

$$\tilde{\sigma}_{\text{prod}\times\text{dec}}^{\text{V}_s\otimes\text{V}_{\text{ew}}} = \int_2 \left[ 2 \text{Re} \left\{ \delta_{\text{V}_{\text{ew}}}^{\text{dec}} \right\} + I^{\text{ew}} \right] d\sigma_{\text{PA}}^0 \otimes \left[ 2 \text{Re} \left\{ \delta_{\text{V}_s}^{V\bar{q}_a q_b} \right\} + \mathbf{I} \right], \quad (2.16)$$

$$\tilde{\sigma}_{\text{prod}\times\text{dec}}^{\text{V}_s\otimes\text{R}_{\text{ew}}} = \iint_{2+\gamma} \left\{ d\sigma_{\text{dec}}^{\text{R}_{\text{ew}}} - \sum_{\substack{I,J \\ I\neq J}} d\sigma_{\text{PA}}^0 \otimes dV_{\text{dip},IJ}^{\text{ew}} \right\} \otimes \left[ 2 \text{Re} \left\{ \delta_{\text{V}_s}^{V\bar{q}_a q_b} \right\} + \mathbf{I} \right], \quad (2.17)$$

where the sum over the emitter–spectator pairs  $(I, J)$  in Eq. (2.17) extends over all particles of the decay subprocess, i.e.  $I, J = \ell_1, \bar{\ell}_2, V$ . We have introduced a compact notation for the QED dipoles,

$$dV_{\text{dip},IJ}^{\text{ew}} = 4\pi\alpha \eta_I Q_I \eta_J Q_J \begin{cases} d_{IV}^{(\text{sub})}, & \text{for } (I = \ell_1, \bar{\ell}_2) \wedge (J = V), \\ g_{IJ}^{(\text{sub})}, & \text{for } (I = \ell_1, \bar{\ell}_2) \wedge (J = \ell_1, \bar{\ell}_2), \\ 0, & \text{for } I = V, \end{cases} \quad (2.18)$$

where  $\eta_i = 1$  for incoming particles and outgoing antiparticles and  $\eta_i = -1$  for incoming antiparticles and outgoing particles. The corresponding endpoint contributions are given by

$$I^{\text{ew}} = \frac{\alpha}{2\pi} Q_{\ell_1} \left[ (Q_{\ell_1} - Q_{\ell_2}) D_{\ell_1 V}^{(\text{sub})} + Q_{\ell_2} G_{\ell_1 \bar{\ell}_2}^{(\text{sub})} \right] + (\ell_1 \leftrightarrow \bar{\ell}_2), \quad (2.19)$$

where the functions  $g^{(\text{sub})}$  and  $G^{(\text{sub})}$  are given in Ref. [87], while  $d^{(\text{sub})}$  and  $D^{(\text{sub})}$  are the decay dipoles and their integrated counterparts constructed in Ref. [90]. Whenever we write  $\ell_1 \leftrightarrow \bar{\ell}_2$ , this implies the interchange  $Q_{\ell_1} \leftrightarrow Q_{\ell_2}$  of the electric charges of the respective fermions, irrespective of their particle or antiparticle nature.

As anticipated in Sect. 2.2.1, all IR singularities contained in  $\delta_{\text{V}_s}^{V\bar{q}_a q_b}$  cancel exactly against the corresponding poles of the  $\mathbf{I}$  operator within the second square bracket of Eq. (2.16). Similarly, all singularities in  $\delta_{\text{V}_{\text{ew}}}^{\text{dec}}$  cancel against the corresponding poles in  $I^{\text{ew}}$  in the first square bracket of Eq. (2.16). As a consequence, it is sufficient to use the correction factors  $\delta_{\text{V}_{\text{ew}}}^{\text{dec}}$  and  $\delta_{\text{V}_s}^{V\bar{q}_a q_b}$  up to  $\mathcal{O}(\epsilon^0)$ . Furthermore, we recall that the correction factors  $\delta_{\text{V}_{\text{ew}}}^{\text{dec}}$  are evaluated at the on-shell point  $p_V^2 = M_V^2$  and, thus, are independent of the phase-space kinematics.

The contributions involving real QCD corrections are given by the third and fourth term in Eq. (2.15). They are obtained by applying the QED dipole subtraction formalism to the sum of the third and fourth line of Eq. (2.14) and result in the following expressions for the IR-finite real-gluon contributions to the cross section,

$$\tilde{\sigma}_{\text{prod}\times\text{dec}}^{\text{R}_s\otimes\text{V}_{\text{ew}}} = \int_3 \left[ 2 \text{Re} \left\{ \delta_{\text{V}_{\text{ew}}}^{\text{dec}} \right\} + I^{\text{ew}} \right] \left\{ d\sigma_{\text{PA}}^{\text{R}_s} - \sum_{\substack{\text{QCD} \\ \text{dipoles}}} d\sigma_{\text{PA}}^0 \otimes dV_{\text{dip}} \right\}, \quad (2.20)$$

$$\tilde{\sigma}_{\text{prod}\times\text{dec}}^{\text{R}_s\otimes\text{R}_{\text{ew}}} = \iint_{3+\gamma} \left\{ d\sigma_{\text{prod}\times\text{dec}}^{\text{R}_s\otimes\text{R}_{\text{ew}}} - \sum_{\substack{\text{QCD} \\ \text{dipoles}}} d\sigma_{\text{dec}}^{\text{R}_{\text{ew}}} \otimes dV_{\text{dip}} - \sum_{\substack{I,J \\ I\neq J}} d\sigma_{\text{PA}}^{\text{R}_s} \otimes dV_{\text{dip},IJ}^{\text{ew}} \right\}$$

$$+ \left. \sum_{\substack{\text{QCD} \\ \text{dipoles}}} \sum_{\substack{I,J \\ I \neq J}} d\sigma_{\text{PA}}^0 \otimes dV_{\text{dip}} \otimes dV_{\text{dip},IJ}^{\text{ew}} \right\}. \quad (2.21)$$

It is instructive to examine the local cancellation of the IR singularities in Eq. (2.21) in more detail. The second term inside the curly brackets of Eq. (2.21) acts as a local counterterm to the double-real emission cross section  $d\sigma^{\text{R}_s \otimes \text{R}_{\text{ew}}}$  in all regions of phase space where the additional QCD radiation becomes unresolved, i.e. soft and/or collinear to the beam. The third term inside the curly brackets of Eq. (2.21) analogously ensures the cancellation of IR singularities in the phase-space regions where the photon becomes soft and/or collinear to a final-state lepton. A subtlety arises in the double-unresolved cases, where the cross sections  $d\sigma_{\text{dec}}^{\text{R}_{\text{ew}}}$  and  $d\sigma_{\text{PA}}^{\text{R}_s}$  become singular as well, and both subtraction terms above will simultaneously act as a local counterterm, leading to the twofold subtraction of the IR singularities. This disparity in the double-unresolved limits is exactly compensated by the last term inside the curly brackets of Eq. (2.21), which therefore has the opposite sign. Note that the evaluation of this last term involves the successive application of two dipole phase-space mappings. Owing to the property of the factorizable initial–final corrections where the emissions in the production and decay stages of the  $V$  boson proceed independently, the two dipole mappings do not interfere with each other and the order in which they are applied is irrelevant. A related property is the factorization of the dipole phase space, where the two one-particle subspaces associated with the two unresolved emissions can be isolated simultaneously. This has the important consequence that the analytic integration over the gluon and photon momenta can be carried out in the same manner as at NLO, which allows us to reuse the known results for the integrated dipoles without modification.

Finally, we consider the convolution terms with additional virtual or real EW corrections given by the last two terms in Eq. (2.15). Since these contributions are essentially given by the lower-order (in  $\alpha_s$ ) cross sections, convoluted with the insertion operators  $\mathbf{K}$  and  $\mathbf{P}$ , they pose no additional complications, and the resulting IR-finite contributions to the cross section can be written as

$$\tilde{\sigma}_{\text{prod} \times \text{dec}}^{\text{C}_s \otimes \text{V}_{\text{ew}}} = \int_0^1 dx \int_2 \left[ 2 \text{Re} \left\{ \delta_{\text{V}_{\text{ew}}}^{\text{dec}} \right\} + I^{\text{ew}} \right] d\sigma_{\text{PA}}^0 \otimes (\mathbf{K} + \mathbf{P}), \quad (2.22)$$

$$\tilde{\sigma}_{\text{prod} \times \text{dec}}^{\text{C}_s \otimes \text{R}_{\text{ew}}} = \int_0^1 dx \int_{2+\gamma} \left\{ d\sigma_{\text{dec}}^{\text{R}_{\text{ew}}} - \sum_{\substack{I,J \\ I \neq J}} d\sigma_{\text{PA}}^0 \otimes dV_{\text{dip},IJ}^{\text{ew}} \right\} \otimes (\mathbf{K} + \mathbf{P}). \quad (2.23)$$

Owing to the Lorentz invariance of the dipole formalism, no special treatment is required in contrast to our calculation of the non-factorizable corrections discussed in Ref. [82], which was carried out with the slicing method to isolate soft-photon singularities.

The results presented so far are appropriate for the case of IR-safe observables, i.e. for the case where collinear photons and leptons are recombined to a “dressed” lepton carrying their total momentum. For non-collinear-safe observables with respect to the final-state leptons, i.e. the treatment of bare muons without photon recombination, we use the method of Ref. [89] and its extension to decay kinematics described in Ref. [90]. The required modifications are described in Appendix C.

## 2.4 Factorizable final–final corrections

The factorizable NNLO corrections of final–final type arise purely from the counterterms to the  $V\ell_1\bar{\ell}_2$  vertex and therefore factorize from the LO matrix element,

$$\delta \mathcal{M}_{\text{V}_s \otimes \text{V}_{\text{ew}}, \text{dec} \times \text{dec}}^{\bar{q}_a q_b \rightarrow \ell_1 \bar{\ell}_2} = \delta_{V\ell_1\bar{\ell}_2}^{\text{ct}, (\alpha_s \alpha)} \mathcal{M}_{0, \text{PA}}^{\bar{q}_a q_b \rightarrow \ell_1 \bar{\ell}_2}. \quad (2.24)$$

The counterterms for the leptonic vector-boson decay only receive contributions from the vector-boson self-energies at  $\mathcal{O}(\alpha_s\alpha)$  [94–99], which enter the counterterms through the vector-boson wave-function renormalization constants and through the renormalization constants of the electromagnetic coupling and the weak-mixing angle. There is only one type of contribution from one-loop diagrams with insertions of one-loop  $\mathcal{O}(\alpha_s)$  or  $\mathcal{O}(\alpha)$  counterterms. It results from massive quark loops in the vector-boson self-energies where the QCD mass renormalization constant has to be taken into account. We make use of the expressions for the vector-boson self-energies of Ref. [99], which include the QCD quark mass counterterm in the on-shell scheme. The expressions for the self-energies in terms of the scalar integrals computed in Ref. [99] are given in Appendix A.

The vertex counterterms in the on-shell renormalization scheme are obtained from the expressions for the corresponding NLO EW counterterms [100] upon replacing the one-loop vector-boson self-energies by the two-loop  $\mathcal{O}(\alpha_s\alpha)$  results and dropping lepton wave-function renormalization constants, which receive no correction at this order. We employ the  $G_\mu$  input-parameter scheme where the electromagnetic coupling constant is derived from the Fermi constant  $G_\mu$  via the relation

$$\alpha_{G_\mu} = \frac{\sqrt{2}}{\pi} G_\mu M_W^2 \left( 1 - \frac{M_W^2}{M_Z^2} \right). \quad (2.25)$$

The counterterm  $\delta Z_e$  for the electromagnetic charge in the  $G_\mu$  scheme is related to the one in the  $\alpha(0)$  input-parameter scheme as follows,

$$\delta Z_e^{G_\mu} = \delta Z_e^{\alpha(0)} - \frac{1}{2} \Delta r. \quad (2.26)$$

The quantity  $\Delta r$  comprises all higher-order corrections to muon decay excluding the contributions that constitute QED corrections in the Fermi model, which are included in the definition of the muon decay constant  $G_\mu$  [101],

$$\Delta r = \left. \frac{\partial \Sigma_T^{AA}(k^2)}{\partial k^2} \right|_{k^2=0} - 2 \frac{\delta s_w}{s_w} + 2 \frac{c_w}{s_w} \frac{\Sigma_T^{AZ}(0)}{M_Z^2} + \frac{\Sigma_T^{WW}(0) - \text{Re} \Sigma_T^{WW}(M_W^2)}{M_W^2} + \delta r, \quad (2.27)$$

with the renormalization constant  $\delta s_w$  of the weak-mixing angle and the transverse parts of the vector-boson self-energies,  $\Sigma_T^{VV'}$ . The  $\mathcal{O}(\alpha_s\alpha)$  contribution to  $\Delta r$  simplifies due to the fact that there is no contribution to the finite remainder  $\delta r$  at this order and the photon–Z-boson mixing self-energy  $\Sigma_T^{AZ}$  vanishes at zero momentum [99]. Moreover, since there are no loop corrections to the leptonic vector-boson decay at  $\mathcal{O}(\alpha_s\alpha)$ , the vertex counterterms are finite. The expressions for the counterterms  $\delta_{V\ell_1\bar{\ell}_2}^{\text{ct},(\alpha_s\alpha)}$  in terms of vector-boson self-energies are explicitly given in Appendix A.

The contribution of the final–final corrections to the cross-section prediction are obtained by a simple phase-space integration over the Born kinematics,

$$\hat{\sigma}_{\text{dec} \times \text{dec}}^{\text{NNLO}_{s \otimes \text{ew}}} = \int_2 2 \text{Re} \left\{ \delta_{V\ell_1\bar{\ell}_2}^{\text{ct},(\alpha_s\alpha)} \right\} d\sigma_{\text{PA}}^0. \quad (2.28)$$

Using the values of the input parameters given in Eq. (3.1) below, the numerical value of the counterterm for the  $W\nu_\ell\bar{\ell}$  vertex is given by

$$\delta_{W\nu_\ell\bar{\ell}}^{\text{ct},(\alpha_s\alpha)} = \frac{\alpha_s \alpha}{\pi^2} \times 0.93. \quad (2.29)$$

The final–final correction to the cross section for the charged-current cross section is therefore below the 0.1% level and phenomenologically negligible. This can be partially attributed to the

choice of the  $G_\mu$ -scheme where universal corrections to charged-current processes are absorbed in the value of  $\alpha_{G_\mu}$ . The numerical values of the counterterms  $\delta_{Z\ell\bar{\ell}}^{\text{ct},\tau,(\alpha_s\alpha)}$  for the  $Z\ell\bar{\ell}$  vertices with lepton chiralities  $\tau = \pm$  are somewhat larger, but of opposite sign:

$$\delta_{Z\ell\bar{\ell}}^{\text{ct},+,( \alpha_s\alpha)} = \frac{\alpha_s \alpha}{\pi^2} \times (-49.3), \quad (2.30a)$$

$$\delta_{Z\ell\bar{\ell}}^{\text{ct},-,( \alpha_s\alpha)} = \frac{\alpha_s \alpha}{\pi^2} \times (+31.8). \quad (2.30b)$$

The resulting corrections to the neutral-current Drell–Yan process are, however, suppressed far below the 0.1% level due to cancellations between the right- and left-handed production channels and are therefore also negligible for all phenomenological purposes.

### 3 Numerical results

In this section we present the numerical results for the dominant mixed QCD–EW corrections to the Drell–Yan process at the LHC for a centre-of-mass energy of  $\sqrt{s} = 14$  TeV. We consider the two processes

$$\begin{aligned} p + p &\rightarrow W^+ \rightarrow \nu_\ell + \ell^+ + X, \\ p + p &\rightarrow Z \rightarrow \ell^- + \ell^+ + X \end{aligned}$$

with electrons or muons in the final state ( $\ell = e, \mu$ ). We further distinguish two alternative treatments of photon radiation: In the “dressed-lepton” case, collinear photon–lepton configurations are treated inclusively using a photon-recombination procedure. As a result, the numerical predictions do not contain large logarithms of the lepton mass, which can be set to zero. The dressed-lepton results are appropriate mostly for electrons in the final state. In the “bare-muon” case, no such recombination is performed, reflecting the experimental situation which allows for the detection of isolated muons. We perform a comparison to naive factorization prescriptions of QCD and EW corrections, as well as to a modelling of photonic final-state radiation (FSR) by structure functions or a photon shower. Moreover, we estimate the impact of the NNLO QCD–EW corrections on the measurement of the W-boson mass.

#### 3.1 Input parameters and event selection

The setup for the calculation is analogous to the one used in Ref. [82]. The choice of input parameters closely follows Ref. [102],

$$\begin{aligned} M_W^{\text{OS}} &= 80.385 \text{ GeV}, & \Gamma_W^{\text{OS}} &= 2.085 \text{ GeV}, \\ M_Z^{\text{OS}} &= 91.1876 \text{ GeV}, & \Gamma_Z^{\text{OS}} &= 2.4952 \text{ GeV}, \\ M_H &= 125.9 \text{ GeV}, & m_t &= 173.07 \text{ GeV}, \\ G_\mu &= 1.1663787 \times 10^{-5} \text{ GeV}^{-2}, & \alpha(0) &= 1/137.035999074, \\ \alpha_s(M_Z) &= 0.119. \end{aligned} \quad (3.1)$$

We convert the on-shell masses and decay widths of the vector bosons to the corresponding pole masses and widths as spelled out in Ref. [82].

The electromagnetic coupling constant used in the LO predictions is obtained from the Fermi constant by Eq. (2.25). In the charged-current process, all relative electroweak corrections are computed using  $\alpha_{G_\mu}$ . In the neutral-current process, however, we follow Ref. [47] and use  $\alpha(0)$

consistently in the relative photonic corrections while the remaining relative weak corrections are proportional to  $\alpha_{G_\mu}$ . The same prescription is applied to the relative  $\mathcal{O}(\alpha_s\alpha)$  corrections.

The masses of the light quark flavours (u, d, c, s, b) and of the leptons are neglected throughout, with the only exception in case of non-collinear-safe observables, where the final-state collinear singularity is regularized by the mass of the muon,

$$m_\mu = 105.658369 \text{ MeV}. \quad (3.2)$$

The CKM matrix is chosen diagonal in the third generation and the mixing between the first two generations is parametrized by the following values for the entries of the quark-mixing matrix,

$$|V_{ud}| = |V_{cs}| = 0.974, \quad |V_{cd}| = |V_{us}| = 0.227. \quad (3.3)$$

For the PDFs we consistently use the NNPDF2.3 sets [103], where the NLO and NNLO QCD–EW corrections are evaluated using the NNPDF2.3QED NLO set [104], which also includes  $\mathcal{O}(\alpha)$  corrections. The value of the strong coupling  $\alpha_s(M_Z)$  quoted in Eq. (3.1) is dictated by the choice of these PDF sets. For the evaluation of the full NLO EW corrections entering the naive products below, we employ the DIS factorization scheme to absorb the mass singularities into the PDFs. The renormalization and factorization scales are set equal, with a fixed value given by the respective gauge-boson mass,

$$\mu_R = \mu_F \equiv \mu = M_V, \quad (3.4)$$

of the process under consideration.

For the experimental identification of the Drell–Yan process we impose the following cuts on the transverse momenta and rapidities of the charged leptons,

$$p_{T,\ell^\pm} > 25 \text{ GeV}, \quad |y_{\ell^\pm}| < 2.5, \quad (3.5)$$

and an additional cut on the missing transverse energy

$$E_T^{\text{miss}} > 25 \text{ GeV}, \quad (3.6)$$

in case of the charged-current process. For the neutral-current process we further require a cut on the invariant mass of the lepton pair,

$$M_{\ell\ell} > 50 \text{ GeV}, \quad (3.7)$$

in order to avoid the photon pole at  $M_{\ell\ell} \rightarrow 0$ .

For the dressed-lepton case, in addition, a photon recombination procedure analogous to the one used in Refs. [39, 47] is applied:

1. Photons close to the beam with a rapidity  $|\eta_\gamma| > 3$  are treated as beam remnants and are not further considered in the event selection.
2. For the photons that pass the first step, the angular distance to the charged leptons  $R_{\ell^\pm\gamma} = \sqrt{(\eta_{\ell^\pm} - \eta_\gamma)^2 + (\phi_{\ell^\pm} - \phi_\gamma)^2}$  is computed, where  $\phi$  denotes the azimuthal angle in the transverse plane. If the distance  $R_{\ell^\pm\gamma}$  between the photon and the closest lepton is smaller than 0.1, the photon is recombined with the lepton by adding the respective four-momenta,  $\ell^\pm(k_i) + \gamma(k) \rightarrow \ell^\pm(k_i + k)$ .
3. Finally, the event selection cuts from Eqs. (3.5)–(3.7) are applied to the resulting event kinematics.



### 3.2 Results for the dominant factorizable corrections

The NNLO QCD–EW corrections to the hadronic Drell–Yan cross section are dominated by the factorizable initial–final  $\mathcal{O}(\alpha_s\alpha)$  corrections,  $\Delta\sigma_{\text{prod}\times\text{dec}}^{\text{NNLO}_s\otimes\text{ew}}$ , which are obtained by convoluting the corresponding partonic corrections  $\hat{\sigma}_{\text{prod}\times\text{dec}}^{\text{NNLO}_s\otimes\text{ew}}$  calculated in Section 2 with the PDFs. Our default prediction for Drell–Yan processes is then obtained by adding these NNLO corrections to the sum of the full NLO QCD and EW corrections,

$$\sigma^{\text{NNLO}_s\otimes\text{ew}} = \sigma^0 + \Delta\sigma^{\text{NLO}_s} + \Delta\sigma^{\text{NLO}_{\text{ew}}} + \Delta\sigma_{\text{prod}\times\text{dec}}^{\text{NNLO}_s\otimes\text{ew}}, \quad (3.8)$$

where all terms are consistently evaluated with the NNPDF2.3QED NLO PDFs. The non-factorizable corrections computed in Ref. [82] were found to have a negligible impact on the cross section and are therefore not included here. Similarly, the factorizable corrections of “final–final” type discussed in Sect. 2.4 turn out to have a negligible impact on the cross-section prediction and are therefore not included in Eq. (3.8) either.

Our result allows to validate estimates of the NNLO QCD–EW corrections based on a naive product ansatz. For this purpose, we define the naive product of the NLO QCD cross section and the relative EW corrections,

$$\begin{aligned} \sigma_{\text{naive fact}}^{\text{NNLO}_s\otimes\text{ew}} &= \sigma^{\text{NLO}_s}(1 + \delta_\alpha) \\ &= \sigma^0 + \Delta\sigma^{\text{NLO}_s} + \Delta\sigma^{\text{NLO}_{\text{ew}}} + \Delta\sigma^{\text{NLO}_s} \delta_\alpha, \end{aligned} \quad (3.9)$$

where the relative EW corrections are defined as the ratio of the NLO EW contribution  $\Delta\sigma^{\text{NLO}_{\text{ew}}}$  with respect to the LO contribution  $\sigma^0$  according to

$$\delta_\alpha \equiv \frac{\Delta\sigma^{\text{NLO}_{\text{ew}}}}{\sigma^0}, \quad (3.10)$$

where both denominator and numerator are evaluated with the same NLO PDFs, so that the EW correction factors are practically independent of the PDFs. In order to compare the factorized expression to the NNLO corrections, we define two different versions of the NLO EW corrections in Eq. (3.10): First, based on the full  $\mathcal{O}(\alpha)$  correction ( $\delta_\alpha$ ), and second, based on the dominant EW final-state correction of the PA ( $\delta_\alpha^{\text{dec}}$ ).

Defining the correction factors,<sup>2</sup>

$$\delta_{\alpha_s}^{\text{prod}\times\text{dec}} \equiv \frac{\Delta\sigma_{\text{prod}\times\text{dec}}^{\text{NNLO}_s\otimes\text{ew}}}{\sigma_{\text{LO}}}, \quad \delta'_{\alpha_s} \equiv \frac{\Delta\sigma^{\text{NLO}_s}}{\sigma_{\text{LO}}}, \quad (3.11)$$

we can cast the relative difference of our best prediction (3.8) and the product ansatz (3.9) into the following form,

$$\frac{\sigma^{\text{NNLO}_s\otimes\text{ew}} - \sigma_{\text{naive fact}}^{\text{NNLO}_s\otimes\text{ew}}}{\sigma_{\text{LO}}} = \delta_{\alpha_s}^{\text{prod}\times\text{dec}} - \delta'_{\alpha_s} \delta_\alpha, \quad (3.12)$$

where the LO prediction  $\sigma^{\text{LO}}$  in the denominators is evaluated with the LO PDFs. The difference of the relative NNLO correction  $\delta_{\alpha_s}^{\text{prod}\times\text{dec}}$  and the naive product  $\delta'_{\alpha_s} \delta_\alpha^{\text{(dec)}}$  therefore allows to assess the validity of a naive product ansatz. As observed in Sect. 2.2, most contributions to the factorizable initial–final corrections take the reducible form of a product of two NLO

---

<sup>2</sup> Note that the correction factor  $\delta'_{\alpha_s}$  differs from that in the standard QCD  $K$  factor  $K_{\text{NLO}_s} = \sigma_{\text{NLO}_s}/\sigma_{\text{LO}} \equiv 1 + \delta_{\alpha_s}$  due to the use of different PDF sets in the Born contributions. See Ref. [92] for further discussion.

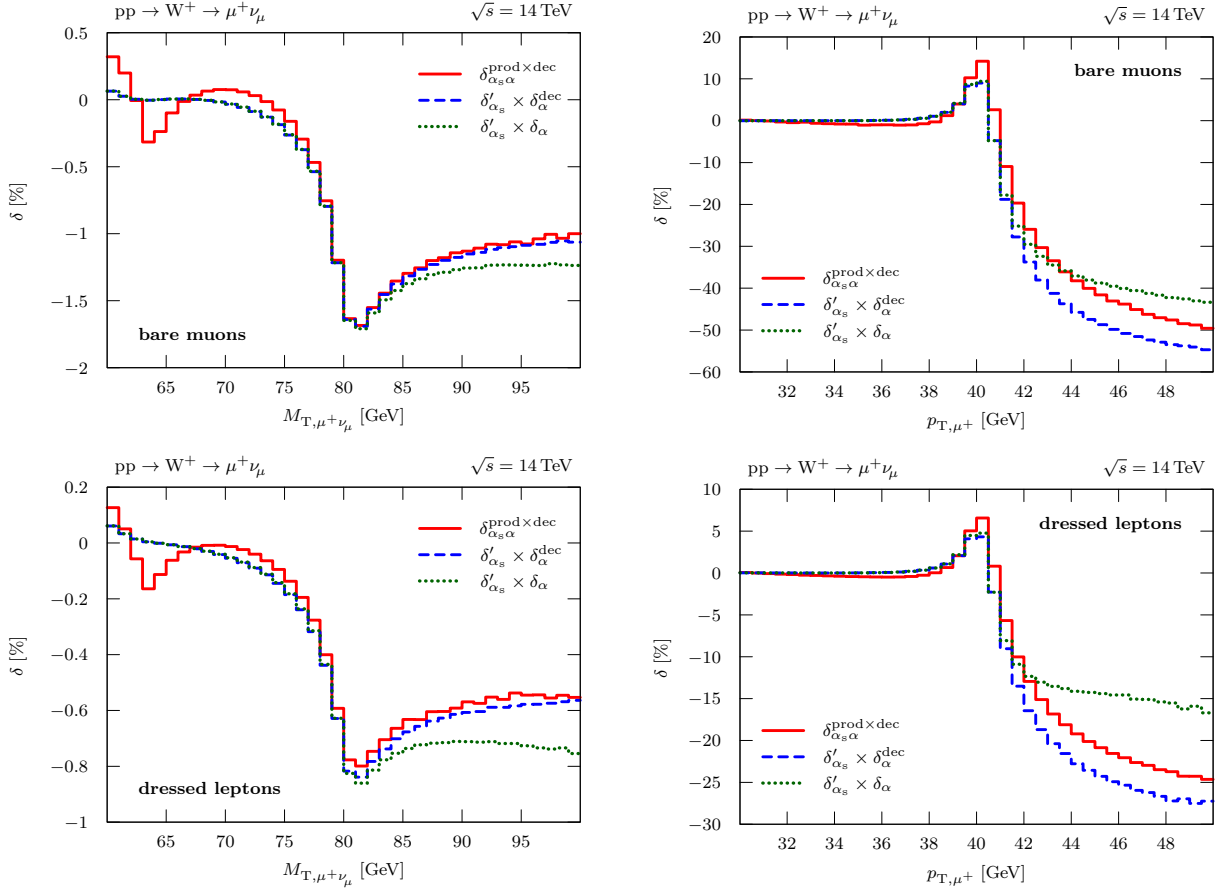


Figure 4: Relative factorizable corrections of  $\mathcal{O}(\alpha_s\alpha)$  induced by initial-state QCD and final-state EW contributions to the transverse-mass (left) and transverse-lepton-momentum (right) distributions for  $W^+$  production at the LHC. The naive products of the NLO correction factors  $\delta'_{\alpha_s}$  and  $\delta_\alpha$  are shown for comparison.

corrections, with the exception of the double-real emission corrections which are defined with the full kinematics of the  $2 \rightarrow 4$  phase space. Note that the double-real contributions are the only ones where the final-state leptons receive recoils from both QCD and photonic radiation, an effect that cannot be captured by naively multiplying NLO QCD and EW corrections. Any large deviations between  $\delta_{\alpha_s\alpha}^{\text{prod}\times\text{dec}}$  and  $\delta'_{\alpha_s} \delta_\alpha^{\text{dec}}$  can therefore be attributed to this type of contribution. The difference of the naive product defined in terms of  $\delta_\alpha^{\text{dec}}$  and  $\delta_\alpha$  allows us to assess the impact of the missing  $\mathcal{O}(\alpha_s\alpha)$  corrections beyond the initial-final corrections considered in our calculation and therefore also provides an error estimate of the PA, and in particular of the omission of the corrections of initial-initial type.

Figure 4 shows the numerical results for the relative  $\mathcal{O}(\alpha_s\alpha)$  initial-final factorizable corrections  $\delta_{\alpha_s\alpha}^{\text{prod}\times\text{dec}}$  to the transverse-mass ( $M_{T,\nu\ell}$ ) and the transverse-lepton-momentum ( $p_{T,\ell}$ ) distributions for  $W^+$  production at the LHC. For  $Z$  production, Figure 5 displays the results for the lepton-invariant-mass ( $M_{\ell\ell}$ ) distribution and a transverse-lepton-momentum ( $p_{T,\ell^+}$ ) distribution. In both figures, the upper plots show the results for bare muons, the lower panels correspond to the corrections with photon recombination. In Figs. 4 and 5 we also compare to the two different implementations of a naive product of correction factors discussed after

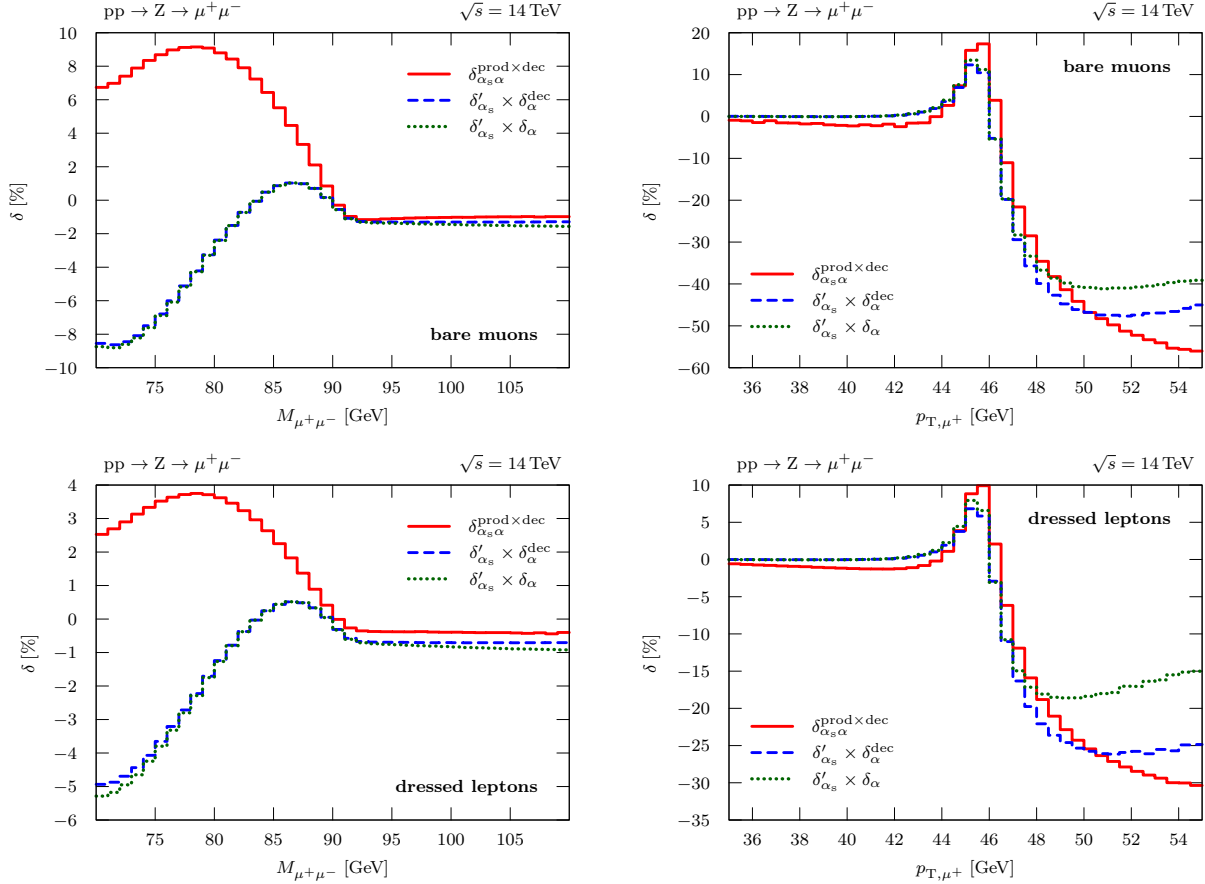


Figure 5: Relative factorizable corrections of  $\mathcal{O}(\alpha_s\alpha)$  induced by initial-state QCD and final-state EW contributions to the lepton-invariant-mass distribution (left) and a transverse-lepton-momentum distribution (right) for Z production at the LHC. The naive products of the NLO correction factors  $\delta'_{\alpha_s}$  and  $\delta_{\alpha}$  are shown for comparison.

Eq. (3.12). In the following, we mainly focus on the results for bare muons. The respective results with photon recombination display the same general features as those for bare muons, but the relative corrections are reduced by approximately a factor of two. This reduction is familiar from NLO EW results and is induced by the cancellation of the collinear singularities by restoring the level of inclusiveness required for the KLN theorem. One observes that the NNLO  $\delta_{\alpha_s\alpha}^{\text{prod}\times\text{dec}}$  corrections are in general better approximated by the simple product ansatz for the case of bare muons than for dressed leptons. This can be understood from the fact that the dominant part of the corrections stem from the collinear logarithms  $\ln(m_{\mu})$  which are known to factorize.

For the  $M_{T,\nu\ell}$  distribution for  $W^+$  production (upper left plot in Fig. 4), the mixed NNLO QCD–EW corrections for bare muons are moderate and amount to approximately  $-1.7\%$  around the resonance, which is about an order of magnitude smaller than the NLO EW corrections.<sup>3</sup>

<sup>3</sup>The structure observed in the correction  $\delta_{\alpha_s\alpha}^{\text{prod}\times\text{dec}}$  around  $M_{T,\nu\ell} \approx 62$  GeV can be attributed to the interplay of the kinematics of the double-real emission corrections and the event selection. It arises close to the kinematic boundary  $M_{T,\nu\ell} > 50$  GeV for the back-to-back kinematics of the non-radiative process implied by the cut  $p_{T,\ell^{\pm}}, E_T^{\text{miss}} > 25$  GeV.

Both variants of the naive product provide a good approximation to the full result in the region around and below the Jacobian peak, which is dominated by resonant W production. For larger values of  $M_{T,\nu\ell}$ , the product  $\delta'_{\alpha_s} \delta_\alpha$  based on the full NLO EW correction factor deviates from the other curves, which signals the growing importance of effects beyond the PA. However, the deviations amount to only few per-mille for  $M_{T,\nu\ell} \lesssim 90$  GeV. The overall good agreement between the  $\delta_{\alpha_s\alpha}^{\text{prod}\times\text{dec}}$  corrections and both naive products can be attributed to well-known insensitivity of the observable  $M_{T,\nu\ell}$  to initial-state radiation effects already seen in the case of NLO corrections in Ref [82].

For the  $p_{T,\ell}$  distributions in the case of bare muons (upper right plots in Figs. 4 and 5, respectively) we observe corrections that are small far below the Jacobian peak, but which rise to about 15% (20%) on the Jacobian peak at  $p_{T,\ell} \approx M_V/2$  for the case of the  $W^+$  boson (Z boson) and then display a steep drop reaching almost  $-50\%$  at  $p_{T,\ell} = 50$  GeV. This enhancement stems from the large QCD corrections above the Jacobian peak familiar from the NLO QCD results (see e.g. Fig. 8 in Ref. [82]) where the recoil due to real QCD radiation shifts events with resonant W/Z bosons above the Jacobian peak. The naive product ansatz fails to provide a good description of the full result  $\delta_{\alpha_s\alpha}^{\text{prod}\times\text{dec}}$  and deviates by 5–10% at the Jacobian peak, where the PA is expected to be the most accurate. This can be attributed to the strong influence of the recoil induced by initial-state radiation on the transverse momentum, which implies a larger effect of the double-real emission corrections on this distribution that are not captured correctly by the naive products. The two versions of the naive products display larger deviations than in the  $M_{T,\nu\ell}$  distribution discussed above, which signals a larger impact of the missing  $\mathcal{O}(\alpha_s\alpha)$  initial–initial corrections. However, these deviations should be interpreted with care, since a fixed-order prediction is not sufficient to describe this distribution around the peak region  $p_{T,\ell} \approx M_V/2$ , which corresponds to the kinematic onset for  $V + \text{jet}$  production and is known to require QCD resummation for a proper description.

In case of the  $M_{\ell\ell}$  distribution for Z production (left-hand plots in Fig. 5), corrections up to 10% are observed below the resonance for the case of bare muons. This is consistent with the large EW corrections at NLO in this region, which arise from final-state photon radiation that shifts the reconstructed value of the invariant lepton-pair mass away from the resonance to lower values. The naive product approximates the full initial–final corrections  $\delta_{\alpha_s\alpha}^{\text{prod}\times\text{dec}}$  reasonably well at the resonance itself ( $M_{\ell\ell} = M_Z$ ) and above, but completely fails already a little below the resonance where the naive products do not even reproduce the sign of the full  $\delta_{\alpha_s\alpha}^{\text{prod}\times\text{dec}}$  correction. This deviation occurs although the invariant-mass distribution is widely unaffected by initial-state radiation effects. The fact that we obtain almost identical corrections from the two versions of the product  $\delta'_{\alpha_s} \delta_\alpha^{\text{dec}}$  and  $\delta'_{\alpha_s} \delta_\alpha$  demonstrates the insensitivity of this observable to photonic initial-state radiation.

In order to locate the source of this large discrepancy we examine the individual correction factors in the naive product in more detail. We restrict ourselves to the case of bare muons and the full NLO EW correction factor  $\delta_\alpha$  for definiteness, which does not affect our conclusions. In Fig. 6(a), we separately plot the two correction factors that enter the naive product  $\delta'_{\alpha_s} \times \delta_\alpha$  and further divide the QCD corrections into the  $q\bar{q}$ - and the  $qg$ -induced contributions. We observe that the two different  $q\bar{q}$ - and  $qg$ -induced channels individually receive large QCD corrections, however, they differ in sign, so that large cancellations take place in the sum  $\delta'_{\alpha_s}$ . A small mismatch in the corrections of the individual channels can therefore quickly lead to a large effect in the QCD corrections which is then further enhanced by the large EW corrections in the product ansatz  $\delta'_{\alpha_s} \times \delta_\alpha$ . Moreover, Figure 6(a) reveals that the QCD correction factor  $\delta'_{\alpha_s}$  is responsible for the sign change at  $M_{\ell\ell} \approx 83$  GeV which is the most striking disagreement of the naive product ansatz with the full factorizable initial–final corrections. This zero crossing happens

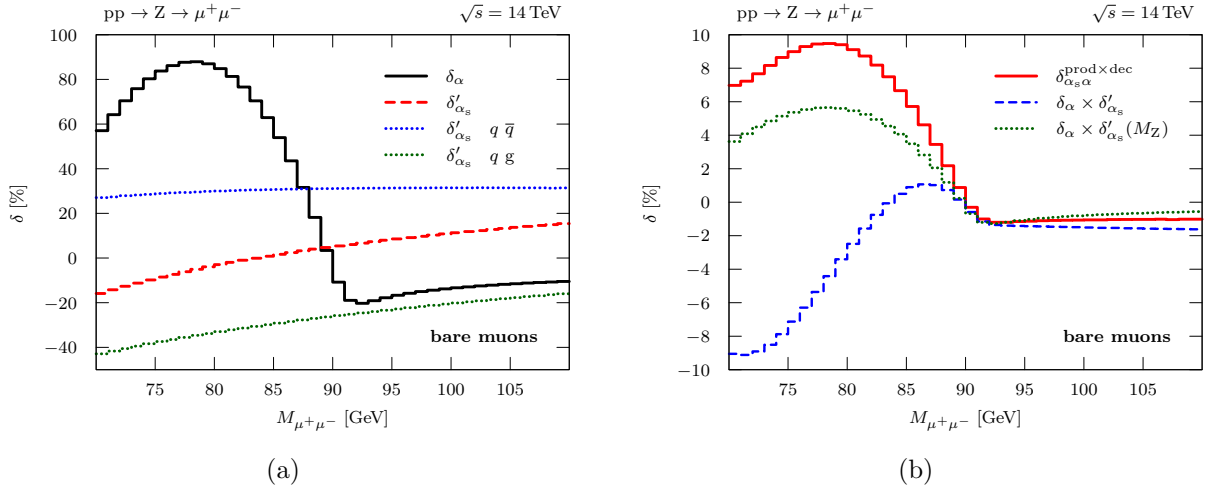


Figure 6: (a) The correction factors to Z-boson production (as shown in the upper left plot of Fig.5) entering the naive product ansatz broken down into its individual contributions with the QCD corrections further divided into the  $q\bar{q}$ - and  $qg$ -induced contributions. (b) A comparison of the corrections shown in the upper left panel of Fig. 5 with the modified product using the value of the QCD corrections at the resonance  $\delta'_{\alpha_s}(M_{\ell\ell} = M_Z) \approx 6.5\%$ .

more than three widths below the resonance where the cross section is reduced by almost two orders of magnitudes compared to the resonance region and, furthermore, will be very sensitive to event selection cuts, since  $\delta'_{\alpha_s}$  arises from the cancellation of two large corrections as we have seen above. In Fig. 6(a) we observe the large EW corrections below the resonance mentioned above, which arise due to the redistribution of events near the Z pole to lower lepton invariant masses by final-state photon radiation. The similar form of the factorizable NNLO initial-final corrections indicates that they mainly stem from an analogous mechanism. This suggests that it is more appropriate to replace the QCD correction factor  $\delta'_{\alpha_s}$  in the naive product by its value at the resonance  $\delta'_{\alpha_s}(M_{\ell\ell} = M_Z) \approx 6.5\%$ , which corresponds to the location of the events that are responsible for the bulk of the large EW corrections below the resonance. In contrast, the naive product ansatz simply multiplies the corrections locally on a bin-by-bin basis. This causes a mismatch in the correction factors and fails to account for the migration of events due to FSR. The comparison of the previous results and the modified product is shown in Fig. 6(b) and clearly shows an improvement despite its very crude construction.

Contrary to the lepton-invariant-mass distribution, the transverse-mass distribution is dominated by events with resonant W bosons even in the range below the Jacobian peak,  $M_{T,\nu\ell} \lesssim M_W$ , so it is less sensitive to the redistribution of events to lower  $M_{T,\nu\ell}$ . This explains why the naive product can provide a good approximation of the full initial-final NNLO corrections. It should be emphasized, however, that even in the case of the  $M_{T,\nu\ell}$  distribution any event selection criteria that deplete events with resonant W bosons below the Jacobian peak will result in increased sensitivity to the effects of FSR and can potentially lead to a failure of a naive product ansatz.

In conclusion, simple approximations in terms of products of correction factors have to be used with care and require a careful case-by-case investigation of their validity.

### 3.3 Leading-logarithmic approximation for final-state photon radiation

As is evident from Figs. 4 and 5, a naive product of QCD and EW correction factors (3.9) is not adequate to approximate the NNLO QCD-EW corrections for all observables. A promising

approach to a factorized approximation for the dominant initial–final corrections can be obtained by combining the full NLO QCD corrections to vector-boson production with the leading-logarithmic (LL) approximation for the final-state corrections. The benefit in this approximation lies in the fact that the interplay of the recoil effects from jet and photon emission is properly taken into account. On the other hand, the logarithmic approximation neglects certain (non-universal) finite contributions, which are, however, suppressed with respect to the dominating radiation effects.

In the structure-function approach [105], the leading-logarithmic approximation of the photonic decay corrections is combined with the NLO QCD corrections to the production by a convolution,

$$\begin{aligned}
\Delta\sigma_{\text{pp,LLFSR}}^{\text{NNLO}_s\otimes\text{ew}} &= \int d\sigma^{\text{NLO}_s}(p_1, p_2; k_1, k_2) \int_0^1 dz_1 \int_0^1 dz_2 \Theta_{\text{cut}}(z_1 k_1) \Theta_{\text{cut}}(z_2 k_2) \\
&\quad \times \left[ \Gamma_{\ell_1 \ell_1}^{\text{LL}}(z_1, Q^2) \Gamma_{\ell_2 \ell_2}^{\text{LL}}(z_2, Q^2) - \delta(1-z_1) \delta(1-z_2) \right] \\
&= \int d\sigma^{\text{NLO}_s}(p_1, p_2; k_1, k_2) \int_0^1 dz_1 \int_0^1 dz_2 \Theta_{\text{cut}}(z_1 k_1) \Theta_{\text{cut}}(z_2 k_2) \\
&\quad \times \left[ \delta(1-z_2) \Gamma_{\ell_1 \ell_1}^{\text{LL},1}(z_1, Q^2) + \delta(1-z_1) \Gamma_{\ell_2 \ell_2}^{\text{LL},1}(z_2, Q^2) + \mathcal{O}(\alpha^2) \right], \tag{3.13}
\end{aligned}$$

where  $d\sigma^{\text{NLO}_s}$  includes the virtual and real QCD corrections. The step function  $\Theta_{\text{cut}}(z_i k_i)$  is equal to 1 if the event passes the cut on the rescaled lepton momentum  $z_i k_i$  and 0 otherwise. The variables  $z_i$  are the momentum fractions describing the respective lepton energy loss by collinear photon emission. For the charged-current process only one of the convolutions is present. The  $\mathcal{O}(\alpha)$  contribution to the structure function  $\Gamma_{\ell\ell}^{\text{LL}}$  reads

$$\Gamma_{\ell\ell}^{\text{LL},1}(z, Q^2) = Q_\ell^2 \frac{\beta_\ell}{4} \left( \frac{1+z^2}{1-z} \right)_+, \tag{3.14}$$

where the large mass logarithm appears in the variable

$$\beta_\ell = \frac{2\alpha}{\pi} \left[ \ln\left(\frac{Q^2}{m_\ell^2}\right) - 1 \right] \tag{3.15}$$

and  $Q_\ell$  denotes the relative electric charge of the lepton  $\ell$ . In order to be consistent in the comparison with our calculation as described in Sect. 3.1, the electromagnetic coupling constant  $\alpha$  appearing in Eq. (3.15) is set to  $\alpha_{G_\mu}$  and  $\alpha(0)$  for the charged-current and neutral-current processes, respectively. The scale  $Q$  is chosen as the gauge-boson mass,

$$Q = M_V, \tag{3.16}$$

and the scale-variation bands shown in the numeric results are obtained by varying the scale by a factor of two up and down from the central scale choice,

$$Q = \xi \cdot M_V, \quad \xi = \frac{1}{2}, 1, 2. \tag{3.17}$$

Since the mass logarithms cancel in observables where photon emission collinear to the final-state charged leptons is treated fully inclusively, the structure-function approach is only applicable to non-collinear-safe observables, i.e. to the bare-muon case.

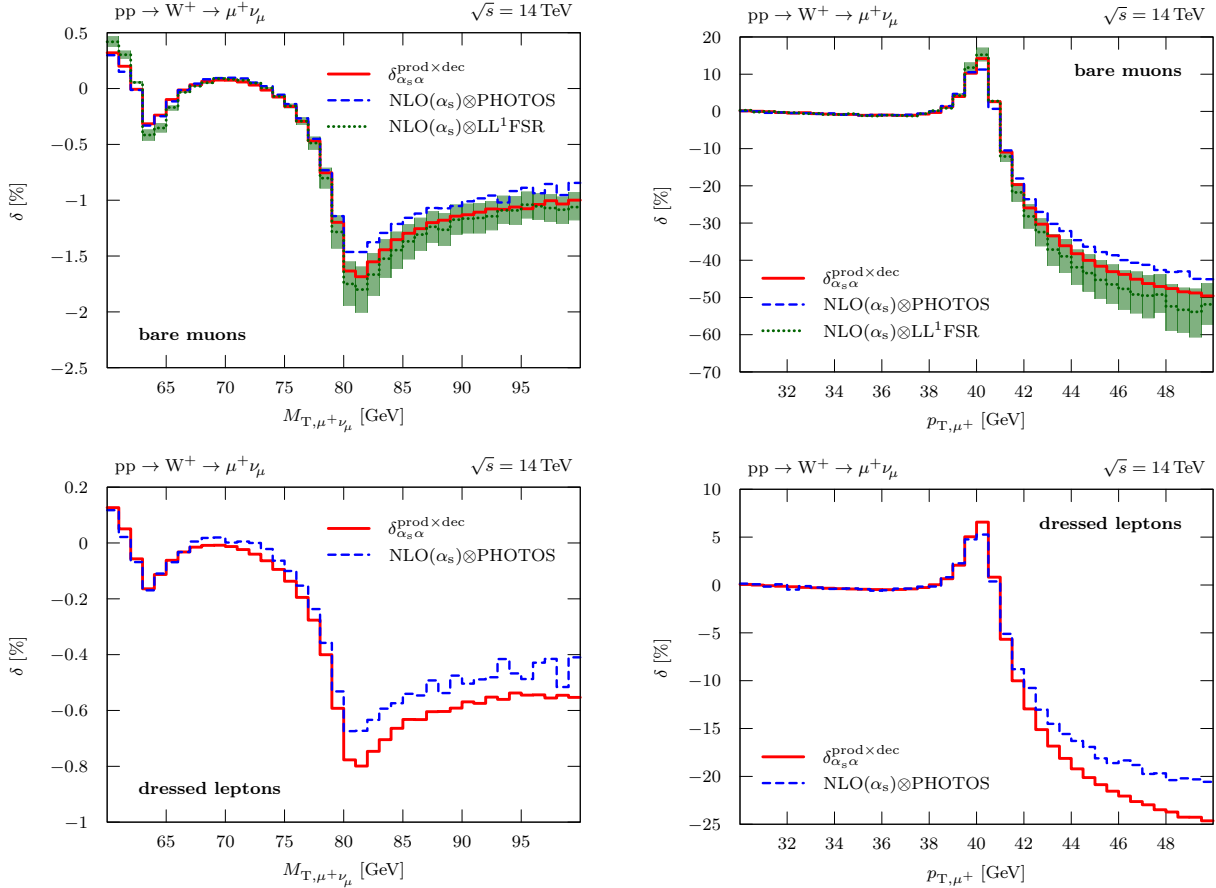


Figure 7: Comparison of the approximation obtained from PHOTOS for the relative  $\mathcal{O}(\alpha_s\alpha)$  initial-state QCD and final-state EW corrections to our best prediction  $\delta_{\alpha_s\alpha}^{\text{prod}\times\text{dec}}$  for the case of the transverse-mass (left) and transverse-lepton-momentum (right) distributions for  $W^+$  production at the LHC, as in Fig. 4. In the bare-muon case, the result (3.13) of the structure-function approach is also shown.

In contrast, in parton-shower approaches to photon radiation (see e.g. Refs. [49, 50, 106]) the photon momenta transverse to the lepton momentum are generated as well, following the differential factorization formula, so that the method is also applicable to the case of collinear-safe observables, i.e. to the dressed-lepton case. For this purpose, we have implemented the combination of the exact NLO QCD prediction for vector-boson production with the simulation of final-state photon radiation using PHOTOS [91]. Since we are interested in comparing to the  $\mathcal{O}(\alpha_s\alpha)$  corrections in our setup, we only generate a single photon emission using PHOTOS and use the same scheme for  $\alpha$  as described in Sect. 3.1. Details on the specific settings within the PHOTOS parton shower are given in Appendix D.

In Figs. 7 and 8 we compare our best prediction (3.8) for the factorizable initial-final  $\mathcal{O}(\alpha_s\alpha)$  corrections to the combination of NLO QCD corrections with the approximate FSR obtained from PHOTOS for the case of  $W^+$  production and Z production, respectively. For the bare-muon case also the result of the structure-function approach according to Eq. (3.13) is shown. The combination of the NLO QCD corrections and approximate FSR leads to a clear improvement compared to the naive product approximations investigated in Section 3.2. This is particularly

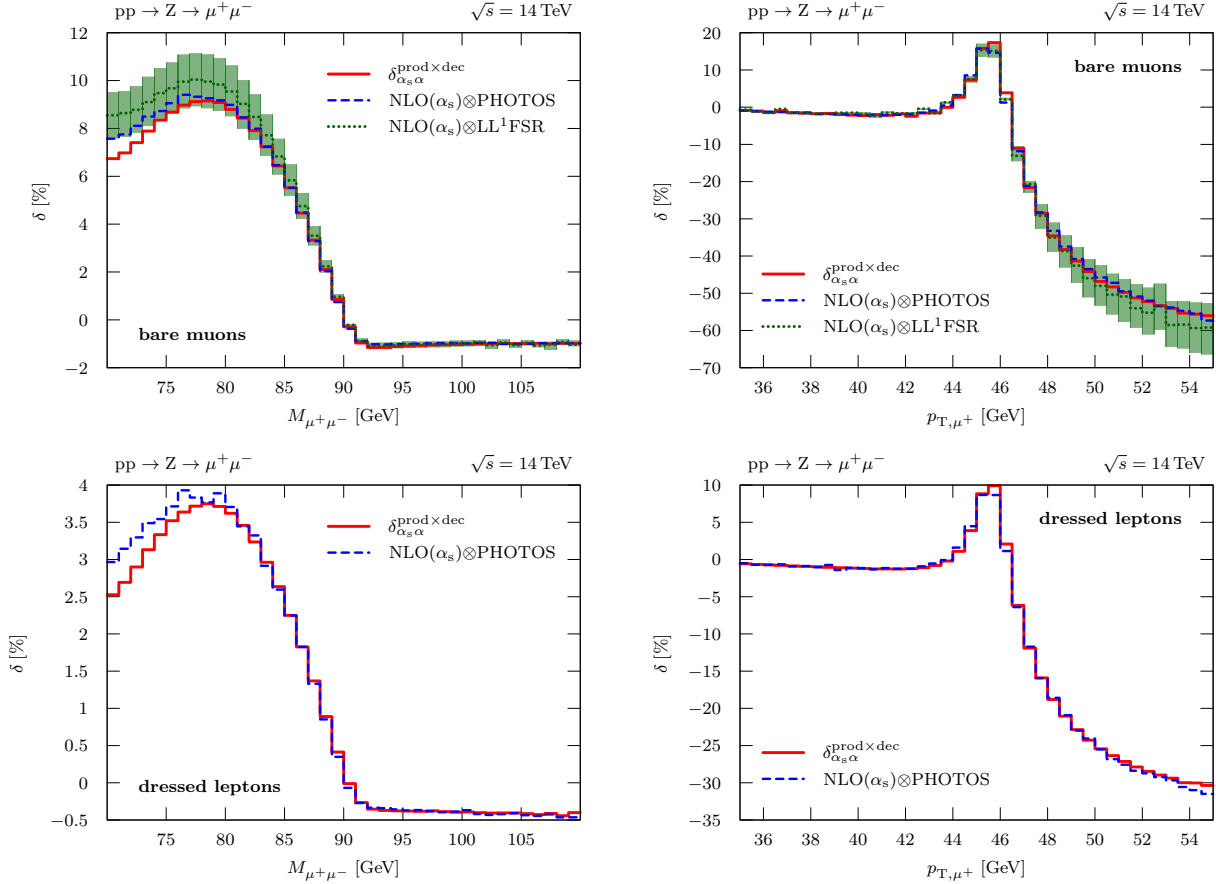


Figure 8: Comparison of the approximation obtained from PHOTOS for the relative  $\mathcal{O}(\alpha_s\alpha)$  initial-state QCD and final-state EW corrections to our best prediction  $\delta_{\alpha_s\alpha}^{\text{prod}\times\text{dec}}$  for the case of the lepton-invariant-mass distribution (left) and a transverse-lepton-momentum distribution (right) for Z production at the LHC, as in Fig. 5. In the bare-muon case, the result (3.13) of the structure-function approach is also shown.

apparent in the neutral-current process where the  $M_{\ell\ell}$  distribution is correctly modelled by both FSR approximations, whereas the naive products shown in Figs. 5 and 6 completely failed to describe this distribution. In the  $M_{T,\nu\ell}$  spectrum of the charged-current process in Fig. 7 one also finds good agreement of the different results below the Jacobian peak and an improvement over the naive product approximations in Fig. 4. The description of the  $p_{T,\ell}$  distributions is also improved compared to the naive product approximations, but some differences remain in the charged-current process.

In spite of the good agreement of the two versions of incorporating final-state-radiation effects, the intrinsic uncertainty of the leading-logarithmic approximations should be kept in mind. For the structure-function approach, this uncertainty is illustrated by the band width resulting from the variation (3.17) of the QED scale  $Q$ . We remark that the multi-photon corrections obtained by employing the un-expanded structure-functions  $\Gamma_{\ell\ell}^{\text{LL}}(z, Q^2)$  in Eq. (3.13) lie well within the aforementioned scale bands, which shows that a proper matching to the full NLO EW calculation is needed to remove the dominant uncertainty of the LL approximation and to predict the higher-order effects reliably. For PHOTOS the intrinsic uncertainty is not shown and not easy to quantify. The good quality of the PHOTOS approximation results from the fact that the finite



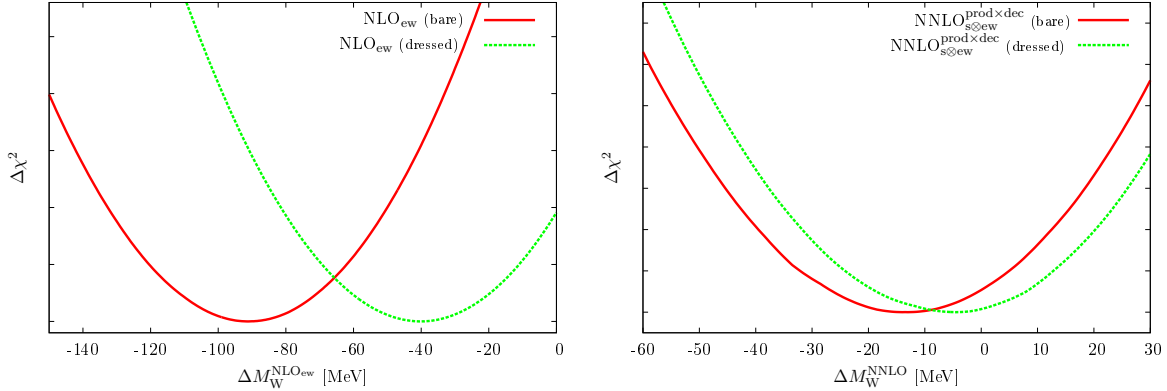


Figure 9: The  $\Delta\chi^2 = \chi^2 - \chi_{\min}^2$  distributions obtained from the fit of the NLO EW corrections (left) and the NNLO production–decay corrections (right) to LO templates in arbitrary units for  $\chi^2$ . The NLO mass shift  $\Delta M_W^{\text{NLO}_{\text{ew}}}$  is given relative to the reference mass  $M_W^{\text{OS}} = 80.385$  GeV, the NNLO shift  $\Delta M_W^{\text{NNLO}}$  is given relative to the output mass of the fit to the sum of the EW and QCD corrections as defined in Eq (3.19).

terms in the photon emission probability are specifically adapted to W/Z-boson decays. The level of agreement with our “full prediction”, thus, cannot be taken over to other processes.

### 3.4 Impact on the W-boson mass extraction

In order to estimate the effect of the  $\mathcal{O}(\alpha_s\alpha)$  corrections on the extraction of the W-boson mass at the LHC we have performed a  $\chi^2$  fit of the  $M_{T,\nu\ell}$  distribution. We treat the  $M_{T,\nu\ell}$  spectra calculated in various theoretical approximations for a reference mass  $M_W^{\text{OS}} = 80.385$  GeV as “pseudo-data” that we fit with “templates” calculated using the LO predictions  $\sigma^0$  (with NLO PDFs) for different values of  $M_W^{\text{OS}}$ . Specifically, we have generated results for 27 transverse-mass bins in the interval  $M_{T,\nu\ell} = [64, 91]$  GeV in steps of 1 GeV, varying the W-boson mass in the interval  $M_W = [80.085, 80.785]$  GeV with steps of  $\Delta M_W = 10$  MeV (steps of  $\Delta M_W = 5$  MeV in the interval  $M_W = [80.285, 80.485]$  GeV). Using a linear interpolation between neighbouring  $M_W$  values, we obtain the integrated cross sections in the  $i$ th  $M_{T,\nu\ell}$  bin,  $\sigma_i^0(M_W)$ , as a continuous function of  $M_W$ . The best-fit value  $M_W^{\text{fit,th}}$  quantifying the impact of a higher-order correction in the theoretical cross section  $\sigma^{\text{th}}$  is then obtained from the minimum of the function

$$\chi^2(M_W^{\text{fit,th}}) = \sum_i \frac{[\sigma_i^{\text{th}}(M_W^{\text{OS}}) - \sigma_i^0(M_W^{\text{fit,th}})]^2}{2\Delta\sigma_i^2}, \quad (3.18)$$

where the sum over  $i$  runs over the transverse-mass bins. Here  $\sigma_i^{\text{th}}$  and  $\sigma_i^0$  are the integrated cross sections in the  $i$ -th bin, uniformly rescaled so that the sum over all 27 bins is identical for all considered cross sections. We assume a statistical error of the pseudo-data and take  $\Delta\sigma_i^2 \propto \sigma_i^{\text{th}}$ . We have also performed a two-parameter fit where the normalization of the templates is fitted simultaneously, leading to identical results. Similarly, allowing the W-boson width in the templates to float and fitting  $M_W$  and  $\Gamma_W$  simultaneously does not significantly affect the estimate of the effect of the  $\mathcal{O}(\alpha_s\alpha)$  corrections on the  $M_W$  measurement.

In the experimental measurements of the transverse-mass distribution, the Jacobian peak is washed out due to the finite energy and momentum resolution of the detectors. In our simple estimate of the impact of higher-order corrections on the extracted value of the W-boson mass,

	bare muons		dressed leptons	
	$M_W^{\text{fit}}$ [GeV]	$\Delta M_W$	$M_W^{\text{fit}}$ [GeV]	$\Delta M_W$
LO	80.385	} - 90 MeV	80.385	} - 40 MeV
NLO <sub>ew</sub>	80.295		80.345	
NLO <sub>s<math>\oplus</math>ew</sub>	80.374	} - 14 MeV	80.417	} - 4 MeV
NNLO	80.360		80.413	

Table 1: Values of the W-boson Mass in GeV obtained from the  $\chi^2$  fit of the  $M_{T,\nu\ell}$  distribution in different theoretical approximations to LO templates and the resulting mass shifts.

we do not attempt to model such effects. We expect the detector effects to affect the different theory predictions in a similar way and to cancel to a large extent in our estimated mass shift, which is obtained from a difference of mass values extracted from pseudo-data calculated using different theory predictions. This assumption is supported by the fact that our estimate of the effect of the NLO EW corrections is similar to the one obtained in Ref. [50] using a Gaussian smearing of the four-momenta to simulate detector effects.

The fit results for several NLO approximations and our best NNLO prediction (3.8) are given in Table 1. To validate our procedure we estimate the mass shift due to the NLO EW corrections by using the prediction  $\sigma^{\text{NLO}_{\text{ew}}} = \sigma^0 + \Delta\sigma^{\text{NLO}_{\text{ew}}}$  as the pseudo-data  $\sigma^{\text{th}}$  in (3.18). The  $\chi^2$  distribution is shown on the left-hand side of Fig. 9 as a function of the mass shift  $\Delta M_W^{\text{NLO}_{\text{ew}}}$  for the dressed-lepton and bare-muon cases. From the minima of the distributions one finds a mass shift of  $\Delta M_W^{\text{NLO}_{\text{ew}}} \approx -90$  MeV for bare muons and  $\Delta M_W^{\text{NLO}_{\text{ew}}} \approx -40$  MeV for dressed muons. These values are comparable to previous results reported in Ref. [50].<sup>4</sup> Alternatively, the effect of the EW corrections can be estimated by comparing the value of  $M_W$  obtained from a fit to the naive product of EW and QCD corrections (3.9) to the result of a fit to the NLO QCD cross section. The results are consistent with the shift estimated from the NLO EW corrections alone.

We have also estimated the effect of multi-photon radiation on the  $M_W$  measurement in the bare-muon case using the structure-function approach given in Eq. (3.13). As discussed in detail in Ref. [46] we match the exponentiated LL-FSR corrections evaluated in the  $\alpha(0)$ -scheme to the NLO calculation in the  $\alpha_{G_\mu}$ -scheme, avoiding double-counting. We obtain a mass shift  $\Delta M_W^{\text{FSR}} \approx 9$  MeV relative to the result of the fit to the NLO EW prediction, which is in qualitative agreement with the result of Ref. [50].

To estimate the impact of the initial-final  $\mathcal{O}(\alpha_s\alpha)$  corrections we consider the mass shift relative to the full NLO result,

$$\Delta M_W^{\text{NNLO}} = M_W^{\text{fit,NNLO}_{s\otimes\text{ew}}^{\text{prod}\times\text{dec}}} - M_W^{\text{fit,NLO}_{s\oplus\text{ew}}} \quad (3.19)$$

<sup>4</sup> In Ref. [50] the values  $\Delta M_W = 110$  MeV (20 MeV) are obtained for the bare-muon (dressed-lepton) case. These values are obtained using the  $\mathcal{O}(\alpha)$ -truncation of a LL shower and for lepton-identification criteria appropriate for the Tevatron taken from Ref. [85], so they cannot be compared directly to our results. In particular, in the dressed-lepton case, a looser recombination criterion  $R_{\ell\pm\gamma} < 0.2$  is applied, which is consistent with a smaller impact of the EW corrections. Note that the role of pseudo-data and templates is reversed in Ref. [50] so that the mass shift has the opposite sign.

where  $M_W^{\text{fit,NNLO}_{s\otimes\text{ew}}^{\text{prod}\times\text{dec}}}$  is the result of using our best prediction (3.8) to generate the pseudo-data, while the sum of the NLO QCD and EW corrections is used for  $\Delta M_W^{\text{fit,NLO}_{s\otimes\text{ew}}}$ . The resulting  $\Delta\chi^2$  distributions for the mass shift are shown in the right-hand plot in Fig. 9. In the bare-muon case, we obtain a mass shift due to  $\mathcal{O}(\alpha_s\alpha)$  corrections of  $\Delta M_W^{\text{NNLO}} \approx -14$  MeV while for the dressed-lepton case we get  $\Delta M_W^{\text{NNLO}} \approx -4$  MeV.

Identical shifts result from replacing the NNLO prediction by the naive product (3.9), which is expected from the good agreement for the  $M_{T,\nu\ell}$ -spectrum in Fig. 4. Using instead the leading-logarithmic approximation of the final-state photon radiation obtained using PHOTOS to compute the  $\mathcal{O}(\alpha_s\alpha)$  corrections, we obtain a mass shift of  $\Delta M_W^{\text{NNLO}} = -11$  MeV ( $-4$  MeV) for the bare-muon (dressed-lepton) case. The effect of the  $\mathcal{O}(\alpha_s\alpha)$  corrections on the mass measurement is therefore of a similar or larger magnitude than the effect of multi-photon radiation. We emphasize that the result  $\Delta M_W^{\text{NNLO}} \approx -14$  MeV is a simple estimate of the impact of the full  $\mathcal{O}(\alpha_s\alpha)$  corrections on the  $M_W$  measurement. The order of magnitude shows that these corrections must be taken into account properly in order to reach the 10 MeV accuracy goal of the LHC experiments. It is beyond the scope of this paper to validate the accuracy of the previous and current theoretical modelling used by the experimental collaborations in the  $M_W$  measurements, which includes the  $\mathcal{O}(\alpha_s\alpha)$  corrections in some approximation.

## 4 Conclusions

The Drell–Yan-like W- and Z-boson production processes are among the most precise probes of the Standard Model and do not only serve as key benchmark or “standard candle” processes, but further allow for precision measurements of the W-boson mass and the effective weak mixing angle. This task of precision physics requires a further increase in the accuracy of the theoretical predictions, where the mixed QCD–electroweak corrections of  $\mathcal{O}(\alpha_s\alpha)$  currently represent the largest unknown component of radiative corrections in terms of fixed-order predictions.

In our previous paper [82] we have established a framework for evaluating the  $\mathcal{O}(\alpha_s\alpha)$  corrections to Drell–Yan processes in the resonance region using the pole approximation and presented the calculation of the so-called non-factorizable corrections. They turned out to be phenomenologically negligible, so that the  $\mathcal{O}(\alpha_s\alpha)$  corrections almost entirely result from factorizable corrections that can be separately attributed to production and decay of the W/Z boson (up to spin correlations).

In this paper we have presented the calculation of the so-called factorizable corrections of “initial–final” and “final–final” types. The latter were calculated in Sect. 2.4 and only comprise finite counterterm contributions which were found to be numerically very small ( $< 0.1\%$ ) and therefore can be safely neglected for all phenomenological purposes. The former, on the other hand, combine large QCD corrections to the production with large EW corrections to the decay subprocesses and are expected to be the dominant contribution of the  $\mathcal{O}(\alpha_s\alpha)$  corrections. Their calculation has been presented in Sect. 2.2, and we have shown numerical results in Sect. 3.2 for the most important observables for the W-boson mass measurement: the transverse-mass and lepton-transverse-momentum distributions for W production. The results for the neutral-current process comprise the invariant-mass and the lepton-transverse-momentum distributions. In the framework of the pole approximation, the only missing  $\mathcal{O}(\alpha_s\alpha)$  corrections are now those of “initial–initial” type. Based on the results of the NLO electroweak calculation, these are expected to be numerically small.

We have used our results for the dominant  $\mathcal{O}(\alpha_s\alpha)$  corrections to test the validity of simpler approximate combinations of EW and QCD corrections: Firstly, we use a naive product ansatz multiplying the NLO QCD and EW correction factors, and secondly, we approximate the  $\mathcal{O}(\alpha_s\alpha)$

contribution by combining leading-logarithmic approximations of QED final-state radiation with the NLO QCD corrections.

We have demonstrated in Sect. 3.2 that naive products fail to capture the factorizable initial–final corrections in distributions such as in the transverse momentum of the lepton, which are sensitive to QCD initial-state radiation and therefore require a correct treatment of the double-real-emission part of the NNLO corrections. Naive products also fail to capture observables that are strongly affected by a redistribution of events due to final-state real-emission corrections, such as the invariant-mass distribution of the neutral-current process. On the other hand, if an observable is less affected by such a redistribution of events or is only affected by it in the vicinity of the resonance, such as the transverse-mass distribution of the charged-current process, the naive products are able to reproduce the factorizable initial–final corrections to a large extent.

In Sect. 3.3 we have investigated to which extent the factorizable initial–final corrections calculated in this paper can be approximated by a combination of the NLO QCD corrections and a collinear approximation of real-photon emission through a QED structure function approach or a QED parton shower such as PHOTOS. For the invariant-mass distribution in Z-boson production we observe a significant improvement in the agreement compared to the naive product ansatz, since both PHOTOS and the QED structure functions model the redistribution of events due to final-state radiation, which is responsible for the bulk of the corrections in this observable. Our results can furthermore be used to validate Monte Carlo event generators where  $\mathcal{O}(\alpha_s\alpha)$  corrections are approximated by a combination of NLO matrix elements and parton showers.

Finally, in Section 3.4 we have illustrated the phenomenological impact of the  $\mathcal{O}(\alpha_s\alpha)$  corrections by estimating the mass shift induced by the factorizable initial–final corrections as  $\approx -14$  MeV for the case of bare muons and  $\approx -4$  MeV for dressed leptons. These corrections therefore have to be properly taken into account in the W-boson mass measurements at the LHC, which aim at a precision of about 10 MeV. It will be interesting to investigate the impact of the  $\mathcal{O}(\alpha_s\alpha)$  corrections on the measurement of the effective weak mixing angle as well in the future.

## Acknowledgement

This project is supported by the German Research Foundation (DFG) via grant DI 784/2-1 and the German Federal Ministry for Education and Research (BMBF). Moreover, A.H. is supported via the ERC Advanced Grant MC@NNLO (340983). C.S. is supported by the Heisenberg Programme of the DFG.

## Appendix

### A Renormalization constants for the leptonic vector-boson decay at $\mathcal{O}(\alpha_s\alpha)$

In this appendix we provide the expressions for the finite  $\mathcal{O}(\alpha_s\alpha)$  counterterms to the leptonic vertices of the W and Z bosons in the on-shell renormalization scheme following the conventions of Ref. [100].

#### A.1 Vector-boson self-energies

The transverse and longitudinal parts of the vector-boson self-energy,  $\Sigma_{\text{T}}^{V_a V_b}$  and  $\Sigma_{\text{L}}^{V_a V_b}$ , are defined by the decomposition of the irreducible two-point function  $\Gamma_{\mu\nu}^{V_a V_b}$  as

$$\Gamma_{\mu\nu}^{V_a V_b}(q) = -i\delta_{ab}g_{\mu\nu}(q^2 - M_{V_a}^2) - i\left(g_{\mu\nu} - \frac{q_\mu q_\nu}{q^2}\right)\Sigma_{\text{T}}^{V_a V_b}(q^2) - i\frac{q_\mu q_\nu}{q^2}\Sigma_{\text{L}}^{V_a V_b}(q^2), \quad (\text{A.1})$$

where  $q$  is the momentum carried by the vector bosons  $V_{a,b}$ . The  $\mathcal{O}(\alpha_s\alpha)$  corrections to the vector-boson self-energies are given in Ref. [99] in terms of scalar functions  $\Pi_T^{V,A}$ .<sup>5</sup> Treating all quarks apart from the top quark as massless, the transverse parts of the vector-boson self-energies can be expressed as follows,

$$\begin{aligned}
\Sigma_T^{WW,(\alpha_s\alpha)}(s) &= \frac{\alpha_s\alpha}{8\pi^2 s_w^2} \left[ 2(\Pi_T^V(s, 0, 0) + \Pi_T^A(s, 0, 0)) + (\Pi_T^V(s, m_t^2, 0) + \Pi_T^A(s, m_t^2, 0)) \right], \\
\Sigma_T^{ZZ,(\alpha_s\alpha)}(s) &= \frac{\alpha_s\alpha}{4\pi^2 s_w^2 c_w^2} \left[ \left( \frac{44}{9} s_w^4 - \frac{14}{3} s_w^2 + \frac{5}{4} \right) \Pi_T^V(s, 0, 0) + \frac{5}{4} \Pi_T^A(s, 0, 0) \right. \\
&\quad \left. + \left( \frac{1}{2} - \frac{4}{3} s_w^2 \right)^2 \Pi_T^V(s, m_t^2, m_t^2) + \frac{1}{4} \Pi_T^A(s, m_t^2, m_t^2) \right], \\
\Sigma_T^{AA,(\alpha_s\alpha)}(s) &= \frac{\alpha_s\alpha}{\pi^2} \left[ \frac{11}{9} \Pi_T^V(s, 0, 0) + \frac{4}{9} \Pi_T^V(s, m_t^2, m_t^2) \right], \\
\Sigma_T^{AZ,(\alpha_s\alpha)}(s) &= -\frac{\alpha_s\alpha}{2\pi^2 s_w c_w} \left[ \left( \frac{7}{6} - \frac{22}{9} s_w^2 \right) \Pi_T^V(s, 0, 0) + \left( \frac{1}{3} - \frac{8}{9} s_w^2 \right) \Pi_T^V(s, m_t^2, m_t^2) \right], \quad (\text{A.2})
\end{aligned}$$

where the explicit expressions for the scalar functions  $\Pi_T^{V,A}$  given in Ref. [99] include the colour factor  $N_c = 3$ . The top-quark mass renormalization is performed in the on-shell scheme.

## A.2 Vertex counterterms

At  $\mathcal{O}(\alpha_s\alpha)$ , the vertex counterterms for the leptonic vector-boson decay receive only contributions from the vector-boson self-energies,

$$\begin{aligned}
\delta_{W\ell_1\bar{\ell}_2}^{\text{ct},(\alpha_s\alpha)} &= \delta Z_e^{(\alpha_s\alpha)} - \frac{\delta s_w^{(\alpha_s\alpha)}}{s_w} + \frac{1}{2} \delta Z_W^{(\alpha_s\alpha)}, \\
\delta_{Z\ell\bar{\ell}}^{\text{ct},\tau_\ell,(\alpha_s\alpha)} &= \frac{\delta g_\ell^{\tau_\ell,(\alpha_s\alpha)}}{g_\ell^{\tau_\ell}} + \frac{1}{2} \delta Z_{ZZ}^{(\alpha_s\alpha)} - \frac{Q_\ell}{2g_\ell^{\tau_\ell}} \delta Z_{AZ}^{(\alpha_s\alpha)}, \quad (\text{A.3})
\end{aligned}$$

where  $\tau_\ell = \pm$  denotes the lepton chirality. The coupling constants entering the Z-boson vertex are given by

$$\begin{aligned}
g_\ell^+ &= -\frac{s_w}{c_w} Q_\ell, & \delta g_\ell^+ &= -\frac{s_w}{c_w} Q_\ell \left[ \delta Z_e + \frac{1}{c_w^2} \frac{\delta s_w}{s_w} \right], \\
g_\ell^- &= \frac{1}{s_w c_w} (I_{w,\ell}^3 - s_w^2 Q_\ell), & \delta g_\ell^- &= \frac{I_{w,\ell}^3}{s_w c_w} \left[ \delta Z_e + \frac{s_w^2 - c_w^2}{c_w^2} \frac{\delta s_w}{s_w} \right] + \delta g_\ell^+, \quad (\text{A.4})
\end{aligned}$$

where  $I_{w,\ell}^3 = -\frac{1}{2}$  is the third component of the weak isospin of the charged lepton  $\ell$ .

---

<sup>5</sup>Note that in the expression given in Eq. (5.4) of Ref. [99] for  $\Pi_T^{V,A}$  in the special case of one vanishing fermion mass, the sign of the term  $1/3(2+\alpha)(\alpha-1)G(x)$  should be reversed in agreement with Ref. [96]. We thank Paolo Gambino for communication on this point.

The vector-boson wave-function renormalization constants can be expressed in terms of the self-energies as follows,

$$\begin{aligned}
\delta Z_{AA} &= - \left. \frac{\partial \Sigma_{\text{T}}^{AA}(k^2)}{\partial k^2} \right|_{k^2=0}, \\
\delta Z_W &= - \text{Re} \left. \frac{\partial \Sigma_{\text{T}}^{WW}(s)}{\partial s} \right|_{s=M_W^2}, & \delta Z_{ZZ} &= - \text{Re} \left. \frac{\partial \Sigma_{\text{T}}^{ZZ}(s)}{\partial s} \right|_{s=M_Z^2}, \\
\delta Z_{ZA} &= 2 \frac{\Sigma_{\text{T}}^{AZ}(0)}{M_Z^2}, & \delta Z_{AZ} &= -2 \text{Re} \frac{\Sigma_{\text{T}}^{AZ}(M_Z^2)}{M_Z^2},
\end{aligned} \tag{A.5}$$

where the  $\mathcal{O}(\alpha_s \alpha)$  contribution to  $\delta Z_{ZA}$  vanishes [99]. The charge-renormalization constant  $\delta Z_e$  in the  $\alpha(0)$  input-parameter scheme is given by

$$\delta Z_e^{\alpha(0)} = -\frac{1}{2} \delta Z_{AA} - \frac{s_w}{c_w} \frac{1}{2} \delta Z_{ZA}. \tag{A.6}$$

The transition to the  $G_\mu$ -scheme is performed according to Eq. (2.26). The renormalization constant for the weak mixing angle is given by

$$\frac{\delta s_w}{s_w} = -\frac{c_w^2}{2s_w^2} \left( \frac{\text{Re} \Sigma_{\text{T}}^{WW}(M_W^2)}{M_W^2} - \frac{\text{Re} \Sigma_{\text{T}}^{ZZ}(M_Z^2)}{M_Z^2} \right). \tag{A.7}$$

The final expressions of the  $\mathcal{O}(\alpha_s \alpha)$  counterterms in the  $G_\mu$ -scheme in terms of self-energies are then given by

$$\begin{aligned}
\delta_{W\ell_1\bar{\ell}_2}^{\text{ct},(\alpha_s\alpha)} &= -\frac{1}{2} \left( \text{Re} \left. \frac{\partial \Sigma_{\text{T}}^{WW,(\alpha_s\alpha)}(s)}{\partial s} \right|_{s=M_W^2} + \frac{\Sigma_{\text{T}}^{WW,(\alpha_s\alpha)}(0) - \text{Re} \Sigma_{\text{T}}^{WW,(\alpha_s\alpha)}(M_W^2)}{M_W^2} \right), \\
\delta_{Z\ell\bar{\ell}}^{\text{ct},+,( \alpha_s\alpha)} &= -\frac{1}{2} \text{Re} \left. \frac{\partial \Sigma_{\text{T}}^{ZZ,(\alpha_s\alpha)}(s)}{\partial s} \right|_{s=M_Z^2} - \left( 1 - \frac{2}{s_w^2} \right) \frac{\text{Re} \Sigma_{\text{T}}^{ZZ,(\alpha_s\alpha)}(M_Z^2)}{2M_Z^2} \\
&\quad - \frac{\Sigma_{\text{T}}^{WW,(\alpha_s\alpha)}(0)}{2M_W^2} + \left( 1 - \frac{1}{s_w^2} \right) \frac{\text{Re} \Sigma_{\text{T}}^{WW,(\alpha_s\alpha)}(M_W^2)}{M_W^2} - \frac{c_w}{s_w} \frac{\text{Re} \Sigma_{\text{T}}^{AZ,(\alpha_s\alpha)}(M_Z^2)}{M_Z^2}, \\
\delta_{Z\ell\bar{\ell}}^{\text{ct},-( \alpha_s\alpha)} &= \delta_{Z\ell\bar{\ell}}^{\text{ct},+,( \alpha_s\alpha)} + \frac{I_{w,f}^3}{s_w c_w g_\ell} \left[ -\frac{2\delta s_w^{(\alpha_s\alpha)}}{s_w} + \frac{c_w}{s_w} \frac{\Sigma_{\text{T}}^{AZ,(\alpha_s\alpha)}(M_Z^2)}{M_Z^2} \right].
\end{aligned} \tag{A.8}$$

## B Explicit form of the IR-safe contributions to the factorizable initial–final corrections

In this section we provide the explicit expressions for each of the contributions to the factorizable initial–final corrections in our master formula (2.15).

The double-virtual corrections (2.16) and the (virtual QCD)  $\times$  (real photonic) corrections (2.17) are obtained by dressing the virtual part of the NLO QCD corrections with the factorizable final-state EW corrections,

$$\tilde{\sigma}_{\bar{q}_a q_b, \text{prod} \times \text{dec}}^{\text{V}_s \otimes \text{V}_{\text{ew}}} = \int_2 \left[ 2 \text{Re} \left\{ \delta_{\text{V}_{\text{ew}}}^{\text{dec}} \right\} + I^{\text{ew}} \right] d\sigma_{\bar{q}_a q_b, \text{PA}}^0 \otimes \left[ 2 \text{Re} \left\{ \delta_{\text{V}_s}^{V \bar{q}_a q_b} \right\} + \mathbf{I} \right], \quad (\text{B.1a})$$

$$\begin{aligned} \tilde{\sigma}_{\bar{q}_a q_b, \text{prod} \times \text{dec}}^{\text{V}_s \otimes \text{R}_{\text{ew}}} = & \iint_{2+\gamma} \left\{ d\sigma_{\text{dec}}^{\text{R}_{\text{ew}}} - 4\pi\alpha \left[ Q_{\ell_1} (Q_{\ell_1} - Q_{\ell_2}) d_{\ell_1 V}^{(\text{sub})} d\sigma_{\bar{q}_a q_b, \text{PA}}^0 \left( \tilde{\Phi}_{2, \ell_1 V} \right) \right. \right. \\ & \left. \left. + Q_{\ell_1} Q_{\ell_2} g_{\ell_1 \bar{\ell}_2}^{(\text{sub})} d\sigma_{\bar{q}_a q_b, \text{PA}}^0 \left( \tilde{\Phi}_{2, \ell_1 \bar{\ell}_2} \right) + (\ell_1 \leftrightarrow \bar{\ell}_2) \right] \otimes \left[ 2 \text{Re} \left\{ \delta_{\text{V}_s}^{V \bar{q}_a q_b} \right\} + \mathbf{I} \right] \right\}, \end{aligned} \quad (\text{B.1b})$$

where the integrated counterpart of the QED dipoles  $I^{\text{ew}}$  is defined in Eq. (2.19). Here  $\tilde{\Phi}_{2, IJ}$  denotes the set of momenta of the two-particle phase space after applying the momentum mapping associated to the dipole  $g_{IJ}^{(\text{sub})}$  or  $d_{IJ}^{(\text{sub})}$ . As in the NLO QCD corrections, only the quark–anti-quark induced channel receives a non-vanishing contribution.

The IR-regularized (real QCD)  $\times$  (virtual EW) corrections (2.20) and the double-real corrections (2.21) are obtained by dressing the real-emission part of the NLO QCD cross sections with the final-state factorizable corrections. Note the two-fold application of the dipole subtraction formalism in case of the double-real corrections. For the quark–anti-quark channel, the explicit expressions are

$$\begin{aligned} \tilde{\sigma}_{\bar{q}_a q_b, \text{prod} \times \text{dec}}^{\text{R}_s \otimes \text{V}_{\text{ew}}} = & \int_3 \left[ 2 \text{Re} \left\{ \delta_{\text{V}_{\text{ew}}}^{\text{dec}} \right\} + I^{\text{ew}} \right] \\ & \times \left\{ d\sigma_{\bar{q}_a q_b, \text{PA}}^{\text{R}_s} - d\sigma_{\bar{q}_a q_b, \text{PA}}^0 \left( \tilde{\Phi}_{n, (\bar{q}_a g) q_b} \right) \otimes dV_{\text{dip}}^{\bar{q}_a, \bar{q}_a} - d\sigma_{\bar{q}_a q_b, \text{PA}}^0 \left( \tilde{\Phi}_{n, (q_b g) \bar{q}_a} \right) \otimes dV_{\text{dip}}^{q_b, q_b} \right\}, \end{aligned} \quad (\text{B.2a})$$

$$\begin{aligned} \tilde{\sigma}_{\bar{q}_a q_b, \text{prod} \times \text{dec}}^{\text{R}_s \otimes \text{R}_{\text{ew}}} = & \iint_{3+\gamma} \left\{ d\sigma_{\bar{q}_a q_b, \text{prod} \times \text{dec}}^{\text{R}_s \otimes \text{R}_{\text{ew}}} \right. \\ & - d\sigma_{\bar{q}_a q_b, \text{dec}}^{\text{R}_{\text{ew}}} \left( \tilde{\Phi}_{2+\gamma, (\bar{q}_a g) q_b} \right) \otimes dV_{\text{dip}}^{\bar{q}_a, \bar{q}_a} - d\sigma_{\bar{q}_a q_b, \text{dec}}^{\text{R}_{\text{ew}}} \left( \tilde{\Phi}_{2+\gamma, (q_b g) \bar{q}_a} \right) \otimes dV_{\text{dip}}^{q_b, q_b} \\ & - 4\pi\alpha \left[ Q_{\ell_1} (Q_{\ell_1} - Q_{\ell_2}) d_{\ell_1 V}^{(\text{sub})} d\sigma_{\bar{q}_a q_b, \text{PA}}^{\text{R}_s} \left( \tilde{\Phi}_{3, \ell_1 V} \right) \right. \\ & \left. + Q_{\ell_1} Q_{\ell_2} g_{\ell_1 \bar{\ell}_2}^{(\text{sub})} d\sigma_{\bar{q}_a q_b, \text{PA}}^{\text{R}_s} \left( \tilde{\Phi}_{3, \ell_1 \bar{\ell}_2} \right) + (\ell_1 \leftrightarrow \bar{\ell}_2) \right] \\ & + 4\pi\alpha \left[ Q_{\ell_1} (Q_{\ell_1} - Q_{\ell_2}) d_{\ell_1 V}^{(\text{sub})} d\sigma_{\bar{q}_a q_b, \text{PA}}^0 \left( \tilde{\Phi}_{2, \ell_1 V} \right) \otimes dV_{\text{dip}}^{\bar{q}_a, \bar{q}_a} \right. \\ & + Q_{\ell_1} (Q_{\ell_1} - Q_{\ell_2}) d_{\ell_1 V}^{(\text{sub})} d\sigma_{\bar{q}_a q_b, \text{PA}}^0 \left( \tilde{\Phi}_{2, \ell_1 V} \right) \otimes dV_{\text{dip}}^{q_b, q_b} \\ & + Q_{\ell_1} Q_{\ell_2} g_{\ell_1 \bar{\ell}_2}^{(\text{sub})} d\sigma_{\bar{q}_a q_b, \text{PA}}^0 \left( \tilde{\Phi}_{2, \ell_1 \bar{\ell}_2} \right) \otimes dV_{\text{dip}}^{\bar{q}_a, \bar{q}_a} \\ & \left. \left. + Q_{\ell_1} Q_{\ell_2} g_{\ell_1 \bar{\ell}_2}^{(\text{sub})} d\sigma_{\bar{q}_a q_b, \text{PA}}^0 \left( \tilde{\Phi}_{2, \ell_1 \bar{\ell}_2} \right) \otimes dV_{\text{dip}}^{q_b, q_b} + (\ell_1 \leftrightarrow \bar{\ell}_2) \right] \right\}. \end{aligned} \quad (\text{B.2b})$$

Here the phase-space kinematics obtained by the successive application of both QCD and EW dipole mappings is denoted by  $\tilde{\Phi}_{2, IJ}^{(ab)c}$ . A detailed discussion of the behaviour of the individual

terms of the double-real corrections in the various singular regions is given in Sect. 2.3. The corresponding expressions for the quark–gluon-initiated subprocesses read

$$\tilde{\sigma}_{gq_b, \text{prod} \times \text{dec}}^{\text{R}_s \otimes \text{V}_{\text{ew}}} = \int_3 \left[ 2 \text{Re} \left\{ \delta_{\text{V}_{\text{ew}}}^{\text{dec}} \right\} + I^{\text{ew}} \right] \left\{ d\sigma_{gq_b, \text{PA}}^{\text{R}_s} - d\sigma_{\bar{q}_a q_b, \text{PA}}^0 \left( \tilde{\Phi}_{n, (gq_a)q_b} \right) \otimes dV_{\text{dip}}^{g, \bar{q}_a} \right\}, \quad (\text{B.3a})$$

$$\begin{aligned} \tilde{\sigma}_{gq_b, \text{prod} \times \text{dec}}^{\text{R}_s \otimes \text{R}_{\text{ew}}} &= \iint_{3+\gamma} \left\{ d\sigma_{gq_b, \text{prod} \times \text{dec}}^{\text{R}_s \otimes \text{R}_{\text{ew}}} - d\sigma_{\bar{q}_a q_b, \text{dec}}^{\text{R}_{\text{ew}}} \left( \tilde{\Phi}_{2+\gamma, (gq_a)q_b} \right) \otimes dV_{\text{dip}}^{g, \bar{q}_a} \right. \\ &\quad - 4\pi\alpha \left[ Q_{\ell_1} (Q_{\ell_1} - Q_{\ell_2}) d_{\ell_1 V}^{(\text{sub})} d\sigma_{gq_b, \text{PA}}^{\text{R}_s} \left( \tilde{\Phi}_{3, \ell_1 V} \right) \right. \\ &\quad \left. \left. + Q_{\ell_1} Q_{\ell_2} g_{\ell_1 \bar{\ell}_2}^{(\text{sub})} d\sigma_{gq_b, \text{PA}}^{\text{R}_s} \left( \tilde{\Phi}_{3, \ell_1 \bar{\ell}_2} \right) + (\ell_1 \leftrightarrow \bar{\ell}_2) \right] \right. \\ &\quad + 4\pi\alpha \left[ Q_{\ell_1} (Q_{\ell_1} - Q_{\ell_2}) d_{\ell_1 V}^{(\text{sub})} d\sigma_{\bar{q}_a q_b, \text{PA}}^0 \left( \tilde{\Phi}_{2, \ell_1 V}^{(gq_a)q_b} \right) \otimes dV_{\text{dip}}^{g, \bar{q}_a} \right. \\ &\quad \left. \left. + Q_{\ell_1} Q_{\ell_2} g_{\ell_1 \bar{\ell}_2}^{(\text{sub})} d\sigma_{\bar{q}_a q_b, \text{PA}}^0 \left( \tilde{\Phi}_{2, \ell_1 \bar{\ell}_2}^{(gq_a)q_b} \right) \otimes dV_{\text{dip}}^{g, \bar{q}_a} + (\ell_1 \leftrightarrow \bar{\ell}_2) \right] \right\}. \quad (\text{B.3b}) \end{aligned}$$

The contribution to the  $g\bar{q}_a$  channel is given in an analogous manner, but is not spelled out explicitly.

The collinear counterterms with additional virtual EW (2.22) and real-photonic (2.23) corrections are constructed from the corresponding term of the NLO QCD corrections by dressing them with the respective factorizable final-state corrections,

$$\begin{aligned} \tilde{\sigma}_{\bar{q}_a q_b, \text{prod} \times \text{dec}}^{\text{C}_s \otimes \text{V}_{\text{ew}}} &= \int_0^1 dx \int_2 \left[ 2 \text{Re} \left\{ \delta_{\text{V}_{\text{ew}}}^{\text{dec}} \right\} + I^{\text{ew}} \right] d\sigma_{\bar{q}_a q_b, \text{PA}}^0 (xp_a, pb) \otimes (\mathbf{K} + \mathbf{P})^{\bar{q}_a, \bar{q}_a} \\ &\quad + \int_0^1 dx \int_2 \left[ 2 \text{Re} \left\{ \delta_{\text{V}_{\text{ew}}}^{\text{dec}} \right\} + I^{\text{ew}} \right] d\sigma_{\bar{q}_a q_b, \text{PA}}^0 (p_a, xp_b) \otimes (\mathbf{K} + \mathbf{P})^{q_b, q_b}, \quad (\text{B.4a}) \end{aligned}$$

$$\begin{aligned} \tilde{\sigma}_{\bar{q}_a q_b, \text{prod} \times \text{dec}}^{\text{C}_s \otimes \text{R}_{\text{ew}}} &= \int_0^1 dx \iint_{2+\gamma} \left\{ d\sigma_{\bar{q}_a q_b, \text{dec}}^{\text{R}_{\text{ew}}} (xp_a, pb) \right. \\ &\quad - 4\pi\alpha \left[ Q_{\ell_1} (Q_{\ell_1} - Q_{\ell_2}) d_{\ell_1 V}^{(\text{sub})} d\sigma_{\bar{q}_a q_b, \text{PA}}^0 \left( \tilde{\Phi}_{2, \ell_1 V} (xp_a, pb) \right) \right. \\ &\quad \left. \left. + Q_{\ell_1} Q_{\ell_2} g_{\ell_1 \bar{\ell}_2}^{(\text{sub})} d\sigma_{\bar{q}_a q_b, \text{PA}}^0 \left( \tilde{\Phi}_{2, \ell_1 \bar{\ell}_2} (xp_a, pb) \right) + (\ell_1 \leftrightarrow \bar{\ell}_2) \right] \right\} \otimes (\mathbf{K} + \mathbf{P})^{\bar{q}_a, \bar{q}_a} \\ &\quad + \int_0^1 dx \iint_{2+\gamma} \left\{ d\sigma_{\bar{q}_a q_b, \text{dec}}^{\text{R}_{\text{ew}}} (p_a, xp_b) \right. \\ &\quad - 4\pi\alpha \left[ Q_{\ell_1} (Q_{\ell_1} - Q_{\ell_2}) d_{\ell_1 V}^{(\text{sub})} d\sigma_{\bar{q}_a q_b, \text{PA}}^0 \left( \tilde{\Phi}_{2, \ell_1 V} (p_a, xp_b) \right) \right. \\ &\quad \left. \left. + Q_{\ell_1} Q_{\ell_2} g_{\ell_1 \bar{\ell}_2}^{(\text{sub})} d\sigma_{\bar{q}_a q_b, \text{PA}}^0 \left( \tilde{\Phi}_{2, \ell_1 \bar{\ell}_2} (p_a, xp_b) \right) + (\ell_1 \leftrightarrow \bar{\ell}_2) \right] \right\} \otimes (\mathbf{K} + \mathbf{P})^{q_b, q_b}. \quad (\text{B.4b}) \end{aligned}$$

The corresponding formulae for the gluon–quark channel read

$$\tilde{\sigma}_{gq_b, \text{prod} \times \text{dec}}^{\text{C}_s \otimes \text{V}_{\text{ew}}} = \int_0^1 dx \int_2 \left[ 2 \text{Re} \left\{ \delta_{\text{V}_{\text{ew}}}^{\text{dec}} \right\} + I^{\text{ew}} \right] d\sigma_{\bar{q}_a q_b, \text{PA}}^0 (xp_g, pb) \otimes (\mathbf{K} + \mathbf{P})^{g, \bar{q}_a}, \quad (\text{B.5a})$$



$$\begin{aligned}
\tilde{\sigma}_{gq_b, \text{prod} \times \text{dec}}^{\text{Cs} \otimes \text{R}_{\text{ew}}} &= \int_0^1 dx \int_{2+\gamma} \left\{ d\sigma_{\bar{q}_a q_b, \text{dec}}^{\text{R}_{\text{ew}}}(xp_g, p_b) \right. \\
&\quad - 4\pi\alpha \left[ Q_{\ell_1} (Q_{\ell_1} - Q_{\ell_2}) d_{\ell_1 V}^{(\text{sub})} d\sigma_{\bar{q}_a q_b, \text{PA}}^0 \left( \tilde{\Phi}_{2, \ell_1 V}(xp_g, p_b) \right) \right. \\
&\quad \left. \left. + Q_{\ell_1} Q_{\ell_2} g_{\ell_1 \bar{\ell}_2}^{(\text{sub})} d\sigma_{\bar{q}_a q_b, \text{PA}}^0 \left( \tilde{\Phi}_{2, \ell_1 \bar{\ell}_2}(xp_g, p_b) \right) + (\ell_1 \leftrightarrow \bar{\ell}_2) \right] \right\} \otimes (\mathbf{K} + \mathbf{P})^{g, \bar{q}_a} \quad (\text{B.5b})
\end{aligned}$$

and analogous expressions for the  $g\bar{q}_a$  channel. Here we have made the dependence on the momenta of the incoming partons explicit in order to indicate which particle undergoes a collinear splitting with the momentum fraction given by the convolution variable  $x$ .

### C Non-collinear-safe observables

In order to treat non-collinear-safe observables with respect to the final-state leptons  $i = \ell_1, \bar{\ell}_2$  following Ref. [89], the  $n$ -particle kinematics in the phase space of the subtraction function is treated as an  $(n+1)$ -particle event with a collinear lepton–photon pair, where the momentum shared between the two collinear particles is controlled by the variable  $z_{iJ}$ ,

$$d\sigma_{\text{PA}}^0 \left( \tilde{\Phi}_{2, iJ} \right) \longrightarrow d\sigma_{\text{PA}}^0 \left( \tilde{\Phi}_{2, iJ} \right) \Theta_{\text{cut}} \left( \tilde{\Phi}_{2, iJ} \mid k_i = z_{iJ} \tilde{k}_i, k = (1 - z_{iJ}) \tilde{k}_i \right), \quad (\text{C.1a})$$

$$d\sigma_{\text{PA}}^{\text{Rs}} \left( \tilde{\Phi}_{3, iJ} \right) \longrightarrow d\sigma_{\text{PA}}^{\text{Rs}} \left( \tilde{\Phi}_{3, iJ} \right) \Theta_{\text{cut}} \left( \tilde{\Phi}_{3, iJ} \mid k_i = z_{iJ} \tilde{k}_i, k = (1 - z_{iJ}) \tilde{k}_i \right), \quad (\text{C.1b})$$

$$d\sigma_{\text{PA}}^0 \left( \tilde{\Phi}_{2, iJ}^{(ab)c} \right) \longrightarrow d\sigma_{\text{PA}}^0 \left( \tilde{\Phi}_{2, iJ}^{(ab)c} \right) \Theta_{\text{cut}} \left( \tilde{\Phi}_{2, iJ}^{(ab)c} \mid \tilde{k}_i = z_{iJ} \tilde{\tilde{k}}_i, \tilde{k} = (1 - z_{iJ}) \tilde{\tilde{k}}_i \right), \quad (\text{C.1c})$$

where we have made explicit the cut function for the computation of observables in the notation. This modification induces additional convolution terms over the distribution  $[\bar{\mathcal{I}}^{\text{ew}}(z)]_+$  with

$$\begin{aligned}
\bar{\mathcal{I}}^{\text{ew}}(z) &= \frac{\alpha}{2\pi} Q_{\ell_1} \left[ (Q_{\ell_1} - Q_{\ell_2}) \bar{\mathcal{D}}_{\ell_1 V}^{(\text{sub})}(z) + Q_{\ell_2} \bar{\mathcal{G}}_{\ell_1 \bar{\ell}_2}^{(\text{sub})}(z) \right] \\
&\quad \times \Theta_{\text{cut}} \left( \tilde{\Phi}_2 \mid k_{\ell_1} = z \tilde{k}_{\ell_1}, k = (1 - z) \tilde{k}_{\ell_1} \right) + (\ell_1 \leftrightarrow \bar{\ell}_2), \quad (\text{C.2})
\end{aligned}$$

which we indicate by the label “ $\bar{\text{R}}_{\text{ew}}$ ”. The contribution with virtual QCD corrections is given by

$$\tilde{\sigma}_{\bar{q}_a q_b, \text{prod} \times \text{dec}}^{\text{Vs} \otimes \bar{\text{R}}_{\text{ew}}} = \int_0^1 dz \int_2 [\bar{\mathcal{I}}^{\text{ew}}(z)]_+ d\sigma_{\bar{q}_a q_b, \text{PA}}^0 \otimes \left[ 2 \text{Re} \left\{ \delta_{\text{Vs}}^V \right\} + \mathbf{I} \right], \quad (\text{C.3})$$

and the real-emission corrections for the quark–anti-quark and gluon–quark induced contributions read

$$\begin{aligned}
\tilde{\sigma}_{\bar{q}_a q_b, \text{prod} \times \text{dec}}^{\text{Rs} \otimes \bar{\text{R}}_{\text{ew}}} &= \int_0^1 dz \int_3 [\bar{\mathcal{I}}^{\text{ew}}(z)]_+ \left\{ d\sigma_{\bar{q}_a q_b, \text{PA}}^{\text{Rs}} - d\sigma_{\bar{q}_a q_b, \text{PA}}^0 \left( \tilde{\Phi}_{n, (\bar{q}_a g) q_b} \right) \otimes dV_{\text{dip}}^{\bar{q}_a, \bar{q}_a} \right. \\
&\quad \left. - d\sigma_{\bar{q}_a q_b, \text{PA}}^0 \left( \tilde{\Phi}_{n, (q_b g) \bar{q}_a} \right) \otimes dV_{\text{dip}}^{q_b, q_b} \right\}, \quad (\text{C.4})
\end{aligned}$$

$$\tilde{\sigma}_{gq_b, \text{prod} \times \text{dec}}^{\text{Rs} \otimes \bar{\text{R}}_{\text{ew}}} = \int_0^1 dz \int_3 [\bar{\mathcal{I}}^{\text{ew}}(z)]_+ \left\{ d\sigma_{gq_b, \text{PA}}^{\text{Rs}} - d\sigma_{\bar{q}_a q_b, \text{PA}}^0 \left( \tilde{\Phi}_{n, (gq_a) q_b} \right) \otimes dV_{\text{dip}}^{g, \bar{q}_a} \right\} \quad (\text{C.5})$$

and analogous terms for the  $g\bar{q}_a$  channel. The  $\mathbf{K}$  and  $\mathbf{P}$  operators contain an additional convolution over the momentum fractions  $x$  of the incoming partons and can be written in the following form,

$$\begin{aligned} \tilde{\sigma}_{\bar{q}_a q_b, \text{prod} \times \text{dec}}^{\text{C}_s \otimes \bar{\mathbf{R}}_{\text{ew}}} = & \int_0^1 dx \int_0^1 dz \int_2 [\bar{\mathcal{I}}^{\text{ew}}(z)]_+ d\sigma_{\bar{q}_a q_b, \text{PA}}^0(xp_a, pb) \otimes (\mathbf{K} + \mathbf{P})^{\bar{q}_a, \bar{q}_a} \\ & + \int_0^1 dx \int_0^1 dz \int_2 [\bar{\mathcal{I}}^{\text{ew}}(z)]_+ d\sigma_{\bar{q}_a q_b, \text{PA}}^0(p_a, xpb) \otimes (\mathbf{K} + \mathbf{P})^{q_b, q_b}, \end{aligned} \quad (\text{C.6})$$

$$\tilde{\sigma}_{g q_b, \text{prod} \times \text{dec}}^{\text{C}_s \otimes \bar{\mathbf{R}}_{\text{ew}}} = \int_0^1 dx \int_0^1 dz \int_2 [\bar{\mathcal{I}}^{\text{ew}}(z)]_+ d\sigma_{\bar{q}_a q_b, \text{PA}}^0(xp_g, pb) \otimes (\mathbf{K} + \mathbf{P})^{g, \bar{q}_a} \quad (\text{C.7})$$

and analogous terms for the  $g\bar{q}_a$  channel. Note that the  $\mathbf{K}$  and  $\mathbf{P}$  operators, in general, contain plus distributions with respect to the variable  $x$ , and the above equations need to be properly evaluated in combination with the plus distribution  $[\bar{\mathcal{I}}^{\text{ew}}(z)]_+$  that acts on the integration variable  $z$ .

## D PHOTOS settings

The results using the PHOTOS parton shower shown in Figs. 7 and 8 of Sect. 3.3 were obtained with version 2.15 of the program and the following options:

```
ISEC=.FALSE.,           ITRE=.FALSE.,           IEXP=.FALSE.,
IFTOP=.FALSE.,         XPHCUT=0.01D0 (default value).
```

These settings restrict the parton shower to *at most one* additional photon emission in order to simulate the impact of  $\mathcal{O}(\alpha)$  corrections. Further settings which differ for the charged-current and neutral-current processes are as follows:

<b>W<math>^\pm</math> production:</b>	<b>Z production:</b>
IFW=.TRUE.,	IFW=.FALSE.,
INTERF=.FALSE.,	INTERF=.TRUE.,
ALPHA= $\alpha_{G_\mu}$ ,	ALPHA= $\alpha(0)$ .

Note that the electromagnetic coupling constant  $\alpha$  is adjusted to the respective value used in our calculation of the initial-final corrections as described in Sect. 3.

## References

- [1] TeV4LHC Working Group, S. Abdullin *et al.*, [arXiv:hep-ph/0608322](#) [[hep-ph](#)].
- [2] TeV4LHC-Top and Electroweak Working Group, C. Gerber *et al.*, [arXiv:0705.3251](#) [[hep-ph](#)].
- [3] M. Boonekamp, F. Chevallier, C. Royon, and L. Schoeffel, *Acta Phys.Polon.* **B40** (2009) 2239, [arXiv:0902.1678](#) [[hep-ph](#)].
- [4] S. Haywood *et al.*, [arXiv:hep-ph/0003275](#) [[hep-ph](#)].
- [5] ATLAS Collaboration, N. Besson, M. Boonekamp, E. Klinkby, S. Mehlhase, and T. Petersen, *Eur.Phys.J.* **C57** (2008) 627, [arXiv:0805.2093](#) [[hep-ex](#)].

- [6] M. Baak *et al.*, [arXiv:1310.6708 \[hep-ph\]](#).
- [7] J. Rojo and A. Vicini in *Community Summer Study 2013: Snowmass on the Mississippi Minneapolis, USA*. 2013. [arXiv:1309.1311 \[hep-ph\]](#).
- [8] S. Quackenbush and Z. Sullivan, *Phys. Rev.* **D92** (2015) 3, 033008, [arXiv:1502.04671 \[hep-ph\]](#).
- [9] G. Bozzi, L. Citelli, and A. Vicini, *Phys. Rev.* **D91** (2015) 11, 113005, [arXiv:1501.05587 \[hep-ph\]](#).
- [10] G. Bozzi, L. Citelli, M. Vesterinen, and A. Vicini, [arXiv:1508.06954 \[hep-ex\]](#).
- [11] R. Hamberg, W. van Neerven, and T. Matsuura, *Nucl.Phys.* **B359** (1991) 343. [Erratum-*ibid.* B **644** (2002) 403].
- [12] R. V. Harlander and W. B. Kilgore, *Phys.Rev.Lett.* **88** (2002) 201801, [arXiv:hep-ph/0201206 \[hep-ph\]](#).
- [13] C. Anastasiou, L. J. Dixon, K. Melnikov, and F. Petriello, *Phys.Rev.* **D69** (2004) 094008, [arXiv:hep-ph/0312266 \[hep-ph\]](#).
- [14] K. Melnikov and F. Petriello, *Phys.Rev.Lett.* **96** (2006) 231803, [arXiv:hep-ph/0603182 \[hep-ph\]](#).
- [15] K. Melnikov and F. Petriello, *Phys.Rev.* **D74** (2006) 114017, [arXiv:hep-ph/0609070 \[hep-ph\]](#).
- [16] S. Catani, L. Cieri, G. Ferrera, D. de Florian, and M. Grazzini, *Phys.Rev.Lett.* **103** (2009) 082001, [arXiv:0903.2120 \[hep-ph\]](#).
- [17] R. Gavin, Y. Li, F. Petriello, and S. Quackenbush, *Comput.Phys.Commun.* **182** (2011) 2388, [arXiv:1011.3540 \[hep-ph\]](#).
- [18] R. Gavin, Y. Li, F. Petriello, and S. Quackenbush, *Comput.Phys.Commun.* **184** (2013) 208, [arXiv:1201.5896 \[hep-ph\]](#).
- [19] S. Moch, J. Vermaseren, and A. Vogt, *Nucl.Phys.* **B726** (2005) 317, [arXiv:hep-ph/0506288 \[hep-ph\]](#).
- [20] E. Laenen and L. Magnea, *Phys.Lett.* **B632** (2006) 270, [arXiv:hep-ph/0508284 \[hep-ph\]](#).
- [21] A. Idilbi and X.-d. Ji, *Phys.Rev.* **D72** (2005) 054016, [arXiv:hep-ph/0501006 \[hep-ph\]](#).
- [22] V. Ravindran and J. Smith, *Phys.Rev.* **D76** (2007) 114004, [arXiv:0708.1689 \[hep-ph\]](#).
- [23] C. Balazs and C. Yuan, *Phys.Rev.* **D56** (1997) 5558, [arXiv:hep-ph/9704258 \[hep-ph\]](#).
- [24] F. Landry, R. Brock, P. M. Nadolsky, and C. Yuan, *Phys.Rev.* **D67** (2003) 073016, [arXiv:hep-ph/0212159 \[hep-ph\]](#).
- [25] G. Bozzi, S. Catani, G. Ferrera, D. de Florian, and M. Grazzini, *Phys.Lett.* **B696** (2011) 207, [arXiv:1007.2351 \[hep-ph\]](#).

- [26] S. Mantry and F. Petriello, Phys.Rev. **D83** (2011) 053007, arXiv:1007.3773 [hep-ph].
- [27] T. Becher, M. Neubert, and D. Wilhelm, JHEP **1202** (2012) 124, arXiv:1109.6027 [hep-ph].
- [28] M. Guzzi, P. M. Nadolsky, and B. Wang, Phys.Rev. **D90** (2014) 1, 014030, arXiv:1309.1393 [hep-ph].
- [29] S. Catani, D. de Florian, G. Ferrera, and M. Grazzini, arXiv:1507.06937 [hep-ph].
- [30] S. Frixione and B. R. Webber, arXiv:hep-ph/0612272 [hep-ph].
- [31] S. Alioli, P. Nason, C. Oleari, and E. Re, JHEP **0807** (2008) 060, arXiv:0805.4802 [hep-ph].
- [32] K. Hamilton, P. Richardson, and J. Tully, JHEP **0810** (2008) 015, arXiv:0806.0290 [hep-ph].
- [33] S. Höche, Y. Li, and S. Prestel, Phys.Rev. **D91** (2015) 7, 074015, arXiv:1405.3607 [hep-ph].
- [34] A. Karlberg, E. Re, and G. Zanderighi, JHEP **1409** (2014) 134, arXiv:1407.2940 [hep-ph].
- [35] S. Alioli, C. W. Bauer, C. Berggren, F. J. Tackmann, and J. R. Walsh, Phys. Rev. **D92** (2015) 9, 094020, arXiv:1508.01475 [hep-ph].
- [36] U. Baur, S. Keller, and W. Sakumoto, Phys.Rev. **D57** (1998) 199, arXiv:hep-ph/9707301 [hep-ph].
- [37] V. Zykunov, Eur.Phys.J.direct **C3** (2001) 9, arXiv:hep-ph/0107059 [hep-ph].
- [38] U. Baur, O. Brein, W. Hollik, C. Schappacher, and D. Wackerroth, Phys.Rev. **D65** (2002) 033007, arXiv:hep-ph/0108274 [hep-ph].
- [39] S. Dittmaier and M. Krämer, Phys. Rev. **D65** (2002) 073007, hep-ph/0109062.
- [40] U. Baur and D. Wackerroth, Phys.Rev. **D70** (2004) 073015, arXiv:hep-ph/0405191 [hep-ph].
- [41] A. Arbuzov *et al.*, Eur.Phys.J. **C46** (2006) 407, arXiv:hep-ph/0506110 [hep-ph].
- [42] C. Carloni Calame, G. Montagna, O. Nicrosini, and A. Vicini, JHEP **0612** (2006) 016, arXiv:hep-ph/0609170 [hep-ph].
- [43] V. Zykunov, Phys.Rev. **D75** (2007) 073019, arXiv:hep-ph/0509315 [hep-ph].
- [44] C. Carloni Calame, G. Montagna, O. Nicrosini, and A. Vicini, JHEP **0710** (2007) 109, arXiv:0710.1722 [hep-ph].
- [45] A. Arbuzov *et al.*, Eur.Phys.J. **C54** (2008) 451, arXiv:0711.0625 [hep-ph].
- [46] S. Brensing, S. Dittmaier, M. Krämer, and A. Mück, Phys.Rev. **D77** (2008) 073006, arXiv:0710.3309 [hep-ph].
- [47] S. Dittmaier and M. Huber, JHEP **1001** (2010) 060, arXiv:0911.2329 [hep-ph].

- [48] U. Baur and T. Stelzer, Phys.Rev. **D61** (2000) 073007, arXiv:hep-ph/9910206 [hep-ph].
- [49] W. Placzek and S. Jadach, Eur.Phys.J. **C29** (2003) 325, arXiv:hep-ph/0302065 [hep-ph].
- [50] C. Carloni Calame, G. Montagna, O. Nicrosini, and M. Treccani, Phys.Rev. **D69** (2004) 037301, arXiv:hep-ph/0303102 [hep-ph].
- [51] A. Arbuzov and R. Sadykov, J.Exp.Theor.Phys. **106** (2008) 488, arXiv:0707.0423 [hep-ph].
- [52] R. Boughezal, Y. Li, and F. Petriello, Phys.Rev. **D89** (2014) 034030, arXiv:1312.3972 [hep-ph].
- [53] J. R. Andersen *et al.*, arXiv:1405.1067 [hep-ph].
- [54] G. Balossini *et al.*, JHEP **1001** (2010) 013, arXiv:0907.0276 [hep-ph].
- [55] Q.-H. Cao and C. Yuan, Phys.Rev.Lett. **93** (2004) 042001, arXiv:hep-ph/0401026 [hep-ph].
- [56] P. Richardson, R. Sadykov, A. Sapronov, M. Seymour, and P. Skands, JHEP **1206** (2012) 090, arXiv:1011.5444 [hep-ph].
- [57] C. Bernaciak and D. Wackerroth, Phys.Rev. **D85** (2012) 093003, arXiv:1201.4804 [hep-ph].
- [58] L. Barzè, G. Montagna, P. Nason, O. Nicrosini, and F. Piccinini, JHEP **1204** (2012) 037, arXiv:1202.0465 [hep-ph].
- [59] Y. Li and F. Petriello, Phys.Rev. **D86** (2012) 094034, arXiv:1208.5967 [hep-ph].
- [60] L. Barzè *et al.*, Eur.Phys.J. **C73** (2013) 2474, arXiv:1302.4606 [hep-ph].
- [61] A. Kotikov, J. H. Kühn, and O. Veretin, Nucl.Phys. **B788** (2008) 47, arXiv:hep-ph/0703013 [HEP-PH].
- [62] W. B. Kilgore and C. Sturm, Phys.Rev. **D85** (2012) 033005, arXiv:1107.4798 [hep-ph].
- [63] R. Bonciani, PoS **EPS-HEP2011** (2011) 365.
- [64] A. Czarnecki and J. H. Kühn, Phys.Rev.Lett. **77** (1996) 3955, arXiv:hep-ph/9608366 [hep-ph].
- [65] D. Kara, Nucl.Phys. **B877** (2013) 683, arXiv:1307.7190.
- [66] J. H. Kühn, A. Kulesza, S. Pozzorini, and M. Schulze, Nucl.Phys. **B727** (2005) 368, arXiv:hep-ph/0507178 [hep-ph].
- [67] J. H. Kühn, A. Kulesza, S. Pozzorini, and M. Schulze, Nucl.Phys. **B797** (2008) 27, arXiv:0708.0476 [hep-ph].
- [68] W. Hollik, T. Kasprzik, and B. Kniehl, Nucl.Phys. **B790** (2008) 138, arXiv:0707.2553 [hep-ph].

- [69] A. Denner, S. Dittmaier, T. Kasprzik, and A. Mück, JHEP **0908** (2009) 075, [arXiv:0906.1656 \[hep-ph\]](#).
- [70] A. Denner, S. Dittmaier, T. Kasprzik, and A. Mück, JHEP **1106** (2011) 069, [arXiv:1103.0914 \[hep-ph\]](#).
- [71] A. Denner, S. Dittmaier, T. Kasprzik, and A. Mück, Eur.Phys.J. **C73** (2013) 2297, [arXiv:1211.5078 \[hep-ph\]](#).
- [72] W. Hollik, B. A. Kniehl, E. S. Scherbakova, and O. L. Veretin, Nucl. Phys. **B900** (2015) 576, [arXiv:1504.07574 \[hep-ph\]](#).
- [73] J. Smith, D. Thomas, and W. van Neerven, Z.Phys. **C44** (1989) 267.
- [74] J. Ohnemus, Phys.Rev. **D47** (1993) 940.
- [75] J. Ohnemus, Phys.Rev. **D51** (1995) 1068, [arXiv:hep-ph/9407370 \[hep-ph\]](#).
- [76] L. J. Dixon, Z. Kunszt, and A. Signer, Nucl.Phys. **B531** (1998) 3, [arXiv:hep-ph/9803250 \[hep-ph\]](#).
- [77] J. M. Campbell and R. K. Ellis, Phys.Rev. **D60** (1999) 113006, [arXiv:hep-ph/9905386 \[hep-ph\]](#).
- [78] D. De Florian and A. Signer, Eur.Phys.J. **C16** (2000) 105, [arXiv:hep-ph/0002138 \[hep-ph\]](#).
- [79] J. M. Campbell, R. K. Ellis, and C. Williams, JHEP **1107** (2011) 018, [arXiv:1105.0020 \[hep-ph\]](#).
- [80] A. Denner, S. Dittmaier, M. Hecht, and C. Pasold, JHEP **1504** (2015) 018, [arXiv:1412.7421 \[hep-ph\]](#).
- [81] A. Denner, S. Dittmaier, M. Hecht, and C. Pasold, [arXiv:1510.08742 \[hep-ph\]](#).
- [82] S. Dittmaier, A. Huss, and C. Schwinn, Nucl.Phys. **B885** (2014) 318, [arXiv:1403.3216 \[hep-ph\]](#).
- [83] R. G. Stuart, Phys. Lett. **B262** (1991) 113.
- [84] D. Wackerroth and W. Hollik, Phys. Rev. **D55** (1997) 6788, [hep-ph/9606398](#).
- [85] U. Baur, S. Keller, and D. Wackerroth, Phys.Rev. **D59** (1999) 013002, [arXiv:hep-ph/9807417 \[hep-ph\]](#).
- [86] S. Catani and M. Seymour, Nucl.Phys. **B485** (1997) 291, [arXiv:hep-ph/9605323 \[hep-ph\]](#).
- [87] S. Dittmaier, Nucl. Phys. **B565** (2000) 69, [hep-ph/9904440](#).
- [88] S. Catani, S. Dittmaier, M. H. Seymour, and Z. Trocsanyi, Nucl.Phys. **B627** (2002) 189, [arXiv:hep-ph/0201036 \[hep-ph\]](#).
- [89] S. Dittmaier, A. Kabelschacht, and T. Kasprzik, Nucl.Phys. **B800** (2008) 146, [arXiv:0802.1405 \[hep-ph\]](#).

- [90] L. Basso, S. Dittmaier, A. Huss, and L. Oggero, [arXiv:1507.04676 \[hep-ph\]](#).
- [91] P. Golonka and Z. Was, *Eur.Phys.J.* **C45** (2006) 97, [arXiv:hep-ph/0506026 \[hep-ph\]](#).
- [92] S. Dittmaier, A. Huss, and C. Schwinn, *PoS* **LL2014** (2014) 045, [arXiv:1405.6897 \[hep-ph\]](#).
- [93] A. Huss, *Mixed QCD-electroweak  $\mathcal{O}(\alpha_s\alpha)$  corrections to Drell-Yan processes in the resonance region*. PhD thesis, Freiburg University, 2014.
- [94] T. Chang, K. Gaemers, and W. van Neerven, *Nucl.Phys.* **B202** (1982) 407.
- [95] A. Djouadi and C. Verzegnassi, *Phys.Lett.* **B195** (1987) 265.
- [96] A. Djouadi, *Nuovo Cim.* **A100** (1988) 357.
- [97] B. A. Kniehl, J. H. Kühn, and R. Stuart, *Phys.Lett.* **B214** (1988) 621.
- [98] B. A. Kniehl, *Nucl.Phys.* **B347** (1990) 86.
- [99] A. Djouadi and P. Gambino, *Phys.Rev.* **D49** (1994) 3499, [arXiv:hep-ph/9309298 \[hep-ph\]](#).
- [100] A. Denner, *Fortsch.Phys.* **41** (1993) 307, [arXiv:0709.1075 \[hep-ph\]](#).
- [101] A. Sirlin, *Phys.Rev.* **D22** (1980) 971.
- [102] Particle Data Group, J. Beringer *et al.*, *Phys.Rev.* **D86** (2012) 010001.
- [103] R. D. Ball *et al.*, *Nucl.Phys.* **B867** (2013) 244, [arXiv:1207.1303 \[hep-ph\]](#).
- [104] NNPDF, R. D. Ball *et al.*, *Nucl.Phys.* **B877** (2013) 2, 290, [arXiv:1308.0598 \[hep-ph\]](#).
- [105] E. A. Kuraev and V. S. Fadin, *Sov. J. Nucl. Phys.* **41** (1985) 466.
- [106] C. M. Carloni Calame, G. Montagna, O. Nicrosini, and M. Treccani, *JHEP* **0505** (2005) 019, [arXiv:hep-ph/0502218 \[hep-ph\]](#).